Doctoral dissertation

Surface Melting of Polycrystalline Ice Thin Films
（氷多結晶薄膜の表面融解に関する研究）

Chen Jialu

Graduate School of Science, Hokkaido University

Department of Cosmosciences

2021. 3

Contents

Abstract

A vast amount of ice exists on the earth, and surface melting of ice forms thin liquid water layers, so-called quasi-liquid layers (QLLs), on ice surfaces even below the melting point (0 °C). Because QLLs govern properties of ice surfaces, surface melting of ice plays crucially important roles in a wide variety of natural phenomena on the earth. To understand such phenomena, unraveling the surface melting of ice is indispensable. In nature, a large proportion of ice is present in a polycrystalline state. Hence, in this work the behavior of QLLs on polycrystalline ice was investigated.

Polycrystalline ice samples were prepared by quenching pure water using liquid N_2. Then the surfaces of the polycrystalline ice thin films thus formed were observed using a laser confocal microscope combined with a differential interference contrast microscope (LCM-DIM). In addition, the growth and sublimation of the polycrystalline ice thin films were monitored using a Linnik interferometer. The presence of QLLs on the polycrystalline ice thin films was proved, for the first time, by observing macroscopic fluidity of QLLs. During observations, temperature of ice samples and water vapor pressure were controlled separately.

Firstly, the behavior of grains in polycrystalline ice thin films was investigated. It was found that some grains exhibited relatively fast grain growth on a time scale of approximately 30 min. To eliminate the effects of the grain growth, the grains that exhibited the relatively fast grain growth was excluded from further investigations of the surface melting of the polycrystalline ice thin films.

Next, the formation of QLLs in grooves of grain boundaries and on grain surfaces was investigated. Polystyrene particles (653 nm in diameter) were used as a probe for monitoring the presence of QLLs in grooves of grain boundaries. Then the author found that with increasing temperature, QLLs, whose volume was sufficient to move the polystyrene particles, preferentially appeared in grooves of grain boundaries at -1.9 ± 0.4 °C. After the appearance of the QLLs in the grooves, the QLLs continued to exist. Water vapor pressure dependency of the appearance of the QLLs in the grooves

demonstrates that QLLs in grooves are formed by melting of grain boundaries to eliminate lattice mismatches between adjacent grains. In addition, the author further increased temperature, and found that droplet-type QLLs appeared on grain surfaces at −0.7 ± 0.2 °C but they disappeared within 5 ± 3 min even though the temperature and water vapor pressure were kept constant. These results suggest that droplet-type QLLs on grain surfaces are a metastable phase, as those on ice single crystals. The author proposed two plausible causes for the disappearance of the QLLs, based on faster growth of grain surfaces and changes in distribution of water vapor pressure in the vicinity of the grain surfaces. Moreover, the author found that thin-layer-type QLLs also appeared on the grain surfaces at temperatures higher than −0.7 ± 0.3 °C.

Finally, the behavior of QLLs was investigated at temperatures very close to the melting point. Then the author found that a large amount of QLLs spontaneously emerged from grain boundaries, and then the QLLs thus formed fully covered the surfaces of the polycrystalline ice thin films at −0.3± 0.1 °C, although ice grains still remained solid (unmelted) beneath the QLLs. Hence, the author concluded that it was not bulk melting. Because basal faces of ice single crystals were not fully covered with QLLs at the same temperature, it was expected that wettability of surfaces of polycrystalline ice thin films is significantly higher than that of basal faces. Interferometry observations suggest that at temperatures just below the melting point, QLLs on polycrystalline ice thin films are formed mainly by the melting of grain boundaries.

The experimental results found in this study clearly demonstrate that the behavior of QLLs on a polycrystalline ice thin film is significantly different from that on an ice single crystal. In particular, the author found that grain boundaries play a more important role in the surface melting of polycrystalline ice than grain surfaces. The author expects that the insights obtained in this study will provide a key to unlocking a wide variety of natural phenomena related to surface melting of ice.

1. Introduction

Ice is one of the most abundant and ubiquitous materials on the earth's surface. Hence phase transitions of ice, such as growth, sublimation, etc., dominate a wide variety of phenomena on the earth. Surface melting, also called premelting, is one of such phase transitions of ice, and occurs at temperatures below the melting point (0 °C). Then solid ice surfaces are covered with thin liquid water films, so called quasi-liquid layers (QLLs). QLLs govern properties of ice surfaces below the melting point. It is well acknowledged that surface melting of ice plays crucially important roles in a wide range of phenomena, including the preparation of a snow man [1], frost heave [2, 3], slipperiness of ice [2, 4], regelation [2, 5], conservation of tissues and foods [6, 7], and electrification of thunderclouds [2]. Therefore, unraveling the surface melting of ice is indispensable for understanding these phenomena.

In nature, a large proportion of ice is present in a polycrystalline state. Although numerous researchers have studied the formation of QLLs on single ice crystals, experimental studies on formation of QLLs on/in polycrystalline ice have been limited. Properties specific to polycrystalline ice, such as grain boundaries and grain surfaces with high crystallographic indices may give significant effects on the formation of QLLs. Hence, understanding the behavior of QLLs on polycrystalline ice is a crucially important issue.

1-1. Early studies on surface melting of ice

Although surface melting of ice was first proposed by Faraday in 1840s [1], it was not until the mid-1980s that QLLs on ice crystal surfaces could be measured experimentally [8]. Since then surface melting of ice has attracted considerable attention, and many experimental studies reported the existence of QLLs on ice surfaces by various methods. As summarized in Table 1, surface melting of ice has been studied by infrared spectroscopy [9], ellipsometry [10, 11], proton channeling [12, 13], X-ray

diffraction [14], photoelectron spectroscopy [15, 16], atomic force microscopy [17-20], etc. under various temperature ranges. Almost all studies demonstrated that the thickness of QLLs increased significantly with increasing temperature.

Method and reference	Minimum temperature for the appearance of QLLs (°C)	Ice crystals ¶
Infrared spectroscopy[9]	-10	N.A.
Ellipsometry[10]	basal: ~0, prism: -10	Single
Ellipsometry[11]	basal: -2, prism: -4	Single
Proton backscattering[13]	-30	Single
Photoelectron spectroscopy[16]	-20	N.A.
Atomic force microscopy[17]	-30	Both
Atomic force microscopy[18]	-17 *	N.A.
Atomic force microscopy[19]	-10 *	Poly
Atomic force microscopy[20]	-36	N.A.
Scanning force microscopy[21]	-13 *	Single
Interfacial force microscopy[22]	-25	N.A.
Glancing-angle X-ray scattering[23]	basal: -13.5, prism: -12.5	Single
X-ray diffraction[14]	-2.1	Both
X-ray diffraction[24]	prism: -10	Single
Optical microscopy[25]	-1	Single

Table 1 Early experimental studies on QLLs (simulation studies were not included)

* Lowest temperature adopted in the study

¶ "Single" and "Poly" show ice single crystals and polycrystals, respectively; "Both" denotes both ice single crystals and polycrystals; "N.A." indicates that information about ice crystals is not available

Figure. 1.1 shows examples of temperature dependence of the thickness of QLLs [25], measured by several methods in the early studies summarized in Table 1. As demonstrated in Fig. 1.1, the thicknesses of QLLs exhibit an enormous discrepancy, as much as two orders of magnitudes. Such variations in the thickness of QLLs probably

resulted from a lack of surface sensitivity, spatial and temporal resolutions, and/or variations of ice samples. Hence, to effectively study QLLs on ice crystal surfaces, the techniques used need to have sufficient surface sensitivity and spatial and temporal resolutions.

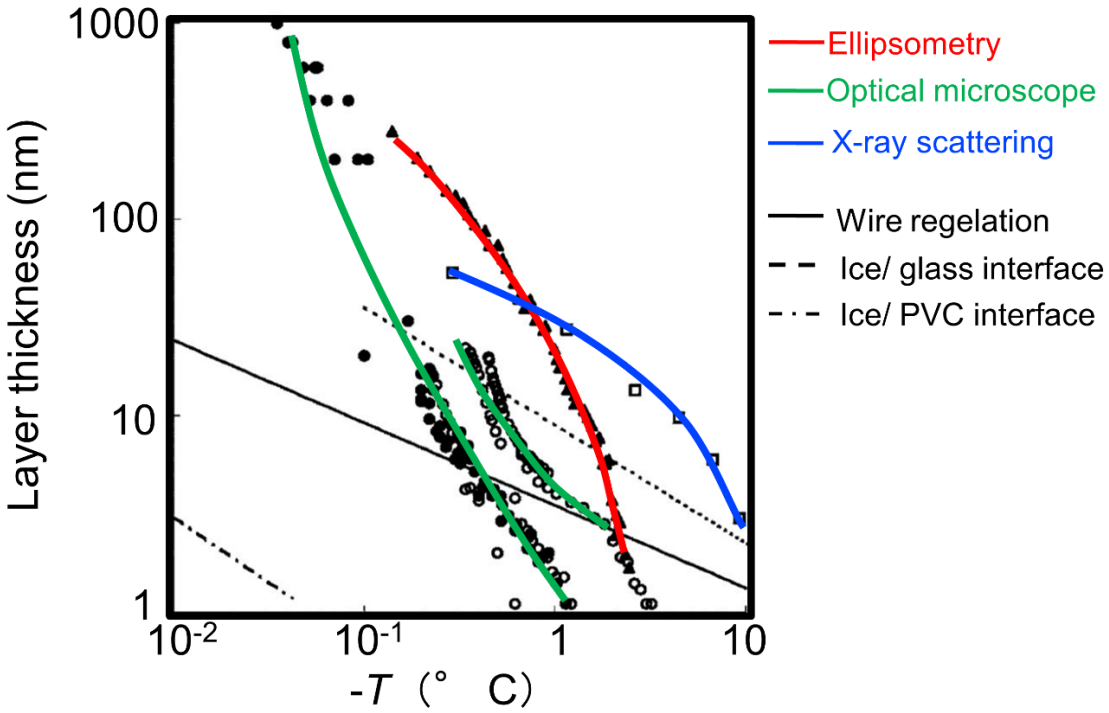

Fig. 1.1. A summary of published data on temperature dependence of thickness of QLLs measured by various methods[2]. Blue, red, and green curves show data obtained by X−ray scattering [23, 24], ellipsometry [10, 11], optical microscopy [25]. The solid line describes the wire regelation experiments [26]. The dashed line derives from experiments on ice/glass interfaces using Pulsed Nuclear Magnetic Resonance (Pulsed NMR) [27] and the dot-dashed line is from experiment on interfacially melted ice/ Polyvinylidene chloride (PVC) interfaces [28].

The existence of QLLs on an ice surface has been also studied from theoretical viewpoint. In the conventional picture of surface melting, it had been thought that only one QLL phase homogeneously covers an ice surface at a solid−vapor equilibrium condition [2]. Lacmann and Stranski first gave a thermodynamic explanation for the wetting of ice c rystal surfaces with QLLs [29]. Then Kuroda and Lacmann further developed this theory [30, 31]. Their theoretical model is based on the competition

between the stabilities of a bulk (unstable) and interfaces (stable) of QLLs (for details, see Appendix A) [30]. When there is no QLL (Fig. 1.2A), there exists one interface between ice and vapor. In contrast, when an ice surface is covered with a QLL (Fig. 1.2B), there exist two interfaces: a QLL−ice interface and a QLL−vapor interface. The free energy of a QLL−ice interface is smaller (more stable) than that of an ice−vapor interface, because the structures of a QLL and an ice are more similar than those of an ice and vapor. In addition, the free energy of a QLL−vapor interface is also smaller (more stable) than that of an ice−vapor interface, for the same reason. Therefore, Kuroda and Lacmann assumed that the sum of the free energies of QLL−ice and QLL−vapor interfaces is smaller (more stable) than the free energy of an ice−vapor interface: an ice crystal surface is always fully wetted with a QLL (complete wetting). Hence, although the bulk free energy of QLLs is higher (less stable) than that of ice crystals, they assumed that a QLL and an ice can be in equilibrium at a solid−vapor equilibrium condition. After these pioneering works, almost all theoretical studies that were published subsequently were based on the same assumption. As explained later in section 1-2-2, because experimental results that are in contradiction with this assumption were found recently, a novel theoretical framework is required.

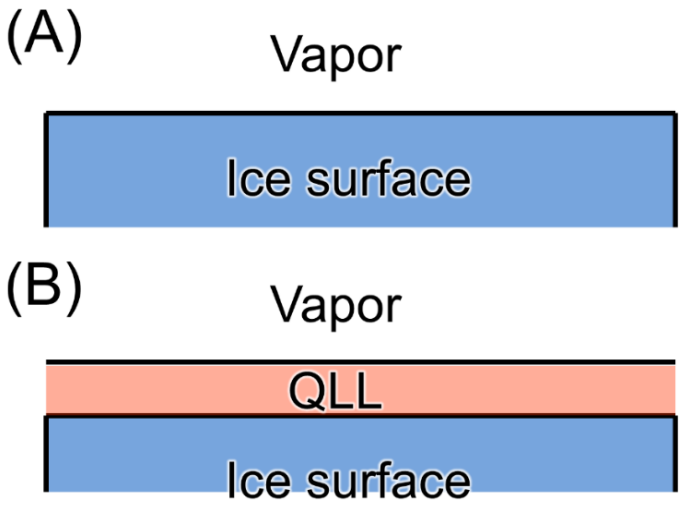

Fig. 1.2. Cross-sectional schematics of (A) a bare ice surface and (B) an ice surface covered with a QLL. The former has only one interface between ice and vapor. In contrast, the latter has two interfaces: a QLL−ice interface and a QLL−vapor interface.

1-2. Recent studies on surface melting of ice single crystals

In order to effectively study the behaviors of a QLL on an ice surface, we need to use experimental techniques that have sufficient surface sensitivity and spatial and temporal resolutions. In the last two decades, several techniques that meet such requirements became newly available. Hence, in this section, we explain recent developments in understanding of QLLs on ice single crystals revealed by such means.

1-2-1. Studies by sum frequency generation (SFG) vibration spectroscopy

Sum frequency generation (SFG) vibration spectroscopy is a powerful tool to study molecular structures of solid/liquid surfaces. Because SFG signals generated from a centrosymmetric medium are canceled out, SFG can obtain signals only from a non-centrosymmetric interface [32]. Therefore, SFG is highly specific and sensitive to a surface, and can detect a topmost layer of a sample surface. In addition, SFG is non-invasive to a sample surface. Therefore, after the pioneering work by the group of Y. R. Shen [33], SFG has been widely used in studying surface properties of ice [34-37].

Recently, by SFG and molecular dynamics simulation Nagata and co-workers studied structures of a topmost molecular layer of a basal face of an ice single crystal [38]. Then they found that above −90 °C the topmost molecular layer becomes disordered (mobile), although below −90 °C the topmost molecular layer shows a crystalline structure. The onset temperature of surface disordering was significantly lower than those measured by other techniques, such as −13.5 °C by glancing-angle X−ray scattering [23], and −2 °C on a basal face by ellipsometry [11], etc., because SFG is significantly more sensitive to disorder of a surface molecular layer than other previous techniques. In addition, Smit and co-workers found that above −16 °C the second topmost molecular layer of a basal face also becomes disordered [39].

Although the thickness of the disordered layers (1-2 molecular layers) is much smaller than those found in the early studies shown in Table 1, researchers working with

SFG believe that the disordered layers can be considered QLLs. They expect that the disordered layer arises from the energetically unstable topmost water molecules due to the interruption of the hydrogen bonding at the topmost layer and is thus homogeneously distributed over the ice surface at the solid−vapor equilibrium condition. To investigate such scenario, further study is necessary to be performed by complementary other methods that have sufficient spatial and temporal resolutions, in addition to the sufficient surface sensitivity.

1-2-2. Studies by advanced optical microscopy

Optical microscopy also showed significant progress during the last two decades. Sazaki and co-workers have developed laser confocal microscopy combined with differential interference contrast microscopy (LCM-DIM) [40], and further improved the sensitivity of LCM-DIM. Then they succeeded in directly visualizing elementary steps (growing ends of ubiquitous molecular layers on a crystal surface) on ice crystal surfaces (0.37 nm in thickness on ice basal faces) [41]. Hence, LCM-DIM has sufficient surface sensitivity and spatial and temporal resolutions to study QLLs on ice crystal surfaces.

By LCM-DIM, Sazaki and coworkers visualized QLLs on ice basal faces for the first time, and found the existence of two types of QLLs with different morphologies (droplets and thin-layers) on ice basal faces [42]. The droplet-type and thin-layer-type QLLs show macroscopic fluidity and are 20 and 200 times more viscous than bulk water, respectively [43]. These QLLs exist also on prism and high-index faces [44], and their formation is induced by dislocations and microdefects [45]. The two different morphologies are caused by wetting transition [46].

The most important result found by LCM-DIM is that the two types of QLLs are a metastable phase and cannot stably exist on ice single crystals in the vicinity of an equilibrium condition of ice and water vapor [46, 47], as shown in Fig. 1.3. In other words, only in pressure-temperature regions (shown in blue and red colors in

supersaturated and undersaturated conditions, respectively, in Fig. 1.3A: a phase diagram of ice (water)), QLLs can exist kinetically on surfaces of ice single crystals [46, 47]. This result is contradicted with those of previous experimental studies by other means and the basic assumption of the theoretical studies explained in the sections 1-1 and 1-2-1.

This discrepancy is likely due to high accuracy in the determination of water vapor pressure by LCM-DIM. Even using interferometry, the accuracy in the determination of a growth/sublimation rate in the direction normal to a crystal surface should be in the order of 1/40 of a wavelength for a minute (10 nm/min). In contrast, because LCM-DIM can visualize the lateral movement of individual elementary steps (0.37 nm in height), the accuracy is higher than the order of several 0.1 nm/min in the normal direction [48, 49]. Therefore, Sazaki and coworkers could precisely determine equilibrium water vapor pressure at a which growth/sublimation rate of an ice single crystal was zero. Consequently, they could find the absence of QLLs in the vicinity of the ice-vapor equilibrium condition. The result shown in Fig. 1.3 clearly demonstrates that there can exist the case in which an ice surface is not fully wetted with a QLL (incomplete wetting), indicating the necessity to develop a novel theoretical framework.

Taking into account the results found by SFG (the section 1-2-1), there still exist open questions. The SFG studies show that the topmost two molecular layers on a basal face are disordered (mobile) in the temperature range shown in Figs. 1.3A. Hence, the relation between the disordered layers and the macroscopically fluidic QLLs is still unknow. In addition, in the observation by LCM-DIM, a basal face grows by a layer-by-layer (solid-like) manner (Fig. 1.3B), although the topmost layer is disordered. To clarify these questions, LCM-DIM observation needs to be performed under much lower temperature range (from −100 to −2 °C), in the future.

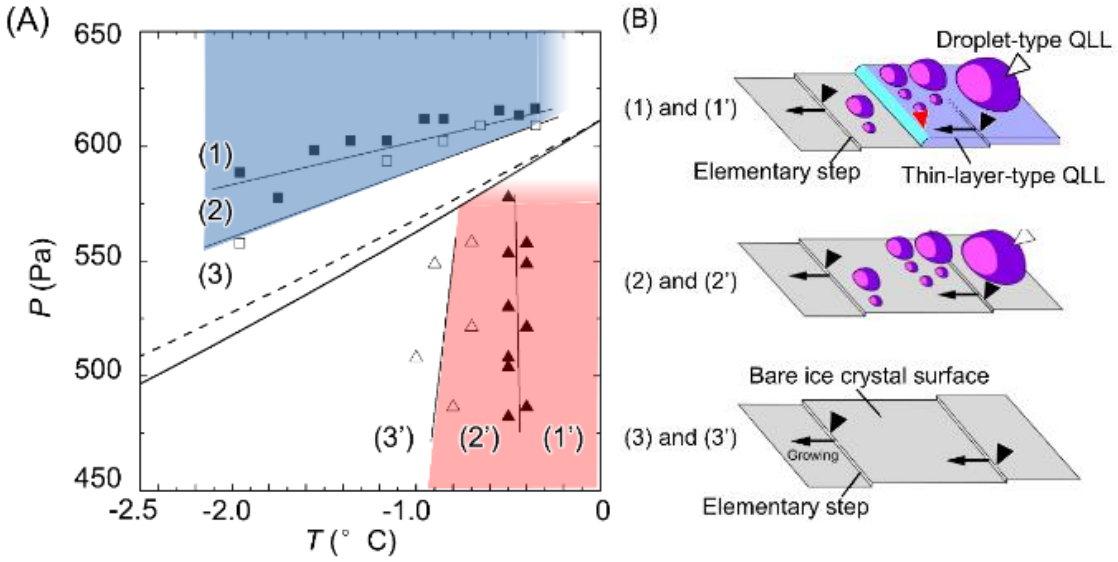

Fig. 1.3. The appearance of macroscopically fluidic QLLs with droplet and thin-layer shapes. (A) A pressure-temperature (*P*-*T*) phase diagram for water and the *P*-*T* regions in which QLLs exist kinetically and continuously on ice single crystals [46, 47]. On surfaces of ice single crystals, open squares (triangles) indicate critical water vapor pressures (temperatures) above which droplet-type QLLs exist kinetically; solid squares (triangles) indicate critical water vapor pressures (temperatures) above which thin-layer-type QLLs exist kinetically. Solid and dotted curves represent the vapor-ice and vapor-liquid water equilibrium curves, respectively. The rightmost and uppermost portions of the blue- and red-colored regions are shown by gradations in colors, respectively, indicating a lack of experimental datum. (B) Schematic illustrations of QLLs and basal faces in the *P*-*T* regions shown in (A). In the regions (1) and (1'), droplet- and thin-layer-type QLLs coexist. In the regions (2) and (2'), only droplet-type QLLs exist. In the regions (3) and (3'), no QLL exists and only a bare surface can be observed.

1-3. Studies on surface melting of polycrystalline ice

A polycrystal is an aggregate of many tiny single crystalline grains. Just after the formation of a polycrystal, single crystalline grains are oriented randomly. This causes specific properties of a polycrystal. A grain boundary is an interface between adjacent grains that have different crystallographic orientations. Hence, a lattice mismatch, which is caused by the contacts of adjacent grains, forms strain energy. Therefore, a grain boundary is significantly more unstable than a bulk of a single crystal. Such instability of a grain boundary provides a driving force for grain growth: as time elapsed, smaller grains disappear and larger grains grow bigger to reduce total area of grain boundaries. In addition, a surface of a grain shows a high crystallographic index. Hence, a grain surface has a significantly higher kink density and thus a higher surface free energy than a low index face. Therefore, such specific properties of a polycrystal are expected to affect the surface melting of polycrystalline ice.

Although numerous experimental studies have been so far performed on surface melting of ice single crystals, experimental studies on surface melting of polycrystalline ice have been very limited. Marder observed the geometries of veins and nodes in polycrystalline ice [50], and studied effects of impurities on the vein width [51]. In addition, two groups studied the behavior of grain boundaries experimentally. Lu et al. studied the diffusion of D_2O in polycrystalline H_2O ice by thermal desorption spectroscopy, and concluded that grain boundary premelting is implausible at temperature as high as −2 °C [52]. Thomson et al. optically measured thin water layers in grain boundaries using bicrystals, and studied the effects of impurities on the thickness of water layers [53, 54]. They found that the thickness of grain boundaries was increased in the range of 1~10 nm with increasing impurity concentration at ~1.5 K undercooling. The relatively small thickness (<10 nm) of grain boundaries indirectly supported the results of Lu et al [52]. However, the agreement with theoretical prediction was not obtained [54]. Furthermore, the abrupt grain boundary melting predicted theoretically[55, 56] has not yet been observed experimentally. Therefore, to obtain a unified understanding, further experimental studies on the behavior of QLLs

on/in polycrystalline ice are highly required.

1-4. Objectives of this study

Revealing surface melting of polycrystalline ice is crucially important in understanding numerous natural phenomena on the earth. Hence, the objective of the present study is to understand surface melting of polycrystalline ice. Surfaces of polycrystalline ice thin films were directly observed by LCM-DIM, which has sufficient surface sensitivity, spatial and temporal resolutions, under various temperature and water vapor pressure. Presence of QLLs on polycrystalline ice thin films was investigated, for the first time, utilizing macroscopic fluidity of QLLs. Growth of ice grains, formation of QLLs in grooves of grain boundaries and that on grain surfaces were investigated. The results were summarized in Chapters 3, 4 and 5.

In Chapter 3, the growth of ice grain was observed by LCM-DIM. Time scale of grain growth was determined at −2.1 °C.

In Chapter 4, the formation of QLLs in grooves of grain boundaries and that on surfaces of ice grains were observed by LCM-DIM at temperature from −2.6 to −0.4 °C. The mechanism of the formation of QLLs was investigated.

In Chapter 5, the formation of QLLs on polycrystalline ice thin films at temperature just below the melting point (from −0.3 to 0 °C) was observed by LCM-DIM. Phenomena observed before bulk melting was investigated.

2. Experiments

In this chapter, we explain experimental details performed in the present study. The section 2-1 presents our optical microscopy system. The section 2-2 shows an observation chamber. The preparation of polycrystalline ice thin films is explained in the section 2-3, and details of the calibration of temperature and water vapor pressure are described in the section 2-4. Finally, the section 2-5 shows how ice surfaces were cleaned using gas flow of pure N_2.

2-1. An observation system

In order to observe polycrystalline ice thin films in-situ, optical microscopy systems were used. The optical microscopy system mainly included a laser confocal microscope, a differential interference contrast microscope, and a Linnik interferometer. In addition, a Michelson interferometer was also used for observation of ice grains.

2-1-1. A laser confocal microscope

In this study, a laser confocal microscope (LCM) (Olympus Corporation, Model FV300) was used. Figure. 2.1 shows a working principle of an LCM. A pinhole functioning as a spatial filter is equipped at a conjugated position of a focal point on a sample surface. Only a light beam reflected from a focal plane (the red light beam in Fig. 2.1) can be focused at the pinhole and then detected by a photomultiplier. In contrast, light beams, reflected from planes other than the focal plane, can be effectively eliminated by the pinhole, as shown by the blue and green light beams. Therefore, the usage of LCM could significantly increase the quality of an image because noises could be efficiently removed.

As explained above, although the use of the pinhole has the significant noise-reduction function, the use of the pinhole significantly decreases the intensity of signal

light. Because a laser has a significantly larger fluence of a light beam than an ordinary halogen lamp, it is widely used as a light source of a confocal microscope: hence it is usually called laser confocal microscopy (LCM).

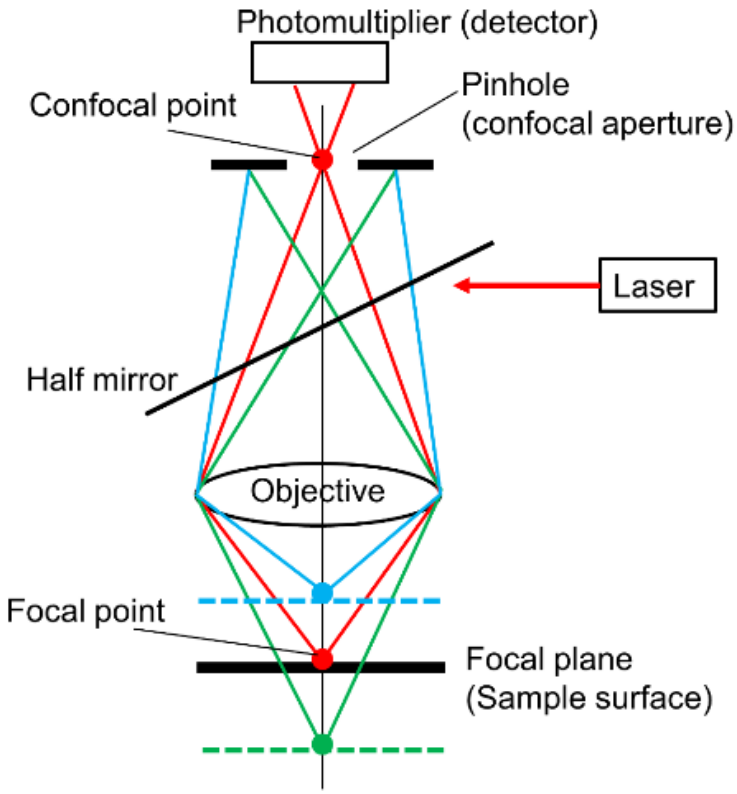

Fig. 2.1. A working principle of a laser confocal microscope (LCM). A super luminescent diode is used as a light source. A pinhole is located at a conjugated position of a focal point on a sample surface. The red light reflected from a focal plane can be focused at the pinhole and then detected by a photomultiplier. In contrast, blue and green light reflected from outside of the focal plane can be eliminated by the pinhole.

2-1-2. A differential interference contrast microscope

In order to detect minute height differences on a sample surface, a differential interference contrast microscope (DIM) of a reflection type was used in this study.

As shown in Fig. 2.2A, a polarized light beam is separated, using a Nomarski prism, into two parallel light beams (ordinary (O-) light and extraordinary (E-) light) with

orthogonal vibrational directions. Then the two parallel light beams are reflected from a sample surface. When a sample surface has a height difference h as schematically shown in Fig. 2.2B, the E- and O-light beams reflected from the sample surface have an optical path difference $2h$. When the reflected light beams finally pass through an analyzer, the E- and O-light beams are subtracted each other by interference (Fig. 2.2B): the optical path difference $2h$ on the left (right) side of the slope on the sample surface is changed into the optical path difference $+2h$ ($-2h$) in the interfered light beam. Then the optical path difference in the interfered light beam is changed into the difference in the intensity utilizing the relation between the optical path difference and interference colors (Fig. 2.2C).

In this study, a superluminescent diode (SLD) with a wavelength of 680 nm (red) was used. Therefore, as shown by a dotted rectangle in Fig. 2.2C, the interference color is changed from black to red with increasing optical path difference. Because the lateral position of the Nomarski prism can be adjusted, the phase difference in the incident E- and O-light beams can be also changed, resulting in the change in the origin of the interference (the zero order interference) from a point O to a point O', as shown schematically in Fig. 2.2C. When the origin of the interference is set at the point O' in Fig. 2.2C, the left (right) side of the slope on the sample surface shows a red (black) color, as shown in Fig. 2.2B. In contrast, a flat sample surface shows a color of the origin O' (intermediate between red and black). As a result, by utilizing the interference, DIM can provide three-dimension like contrast on the sample surface.

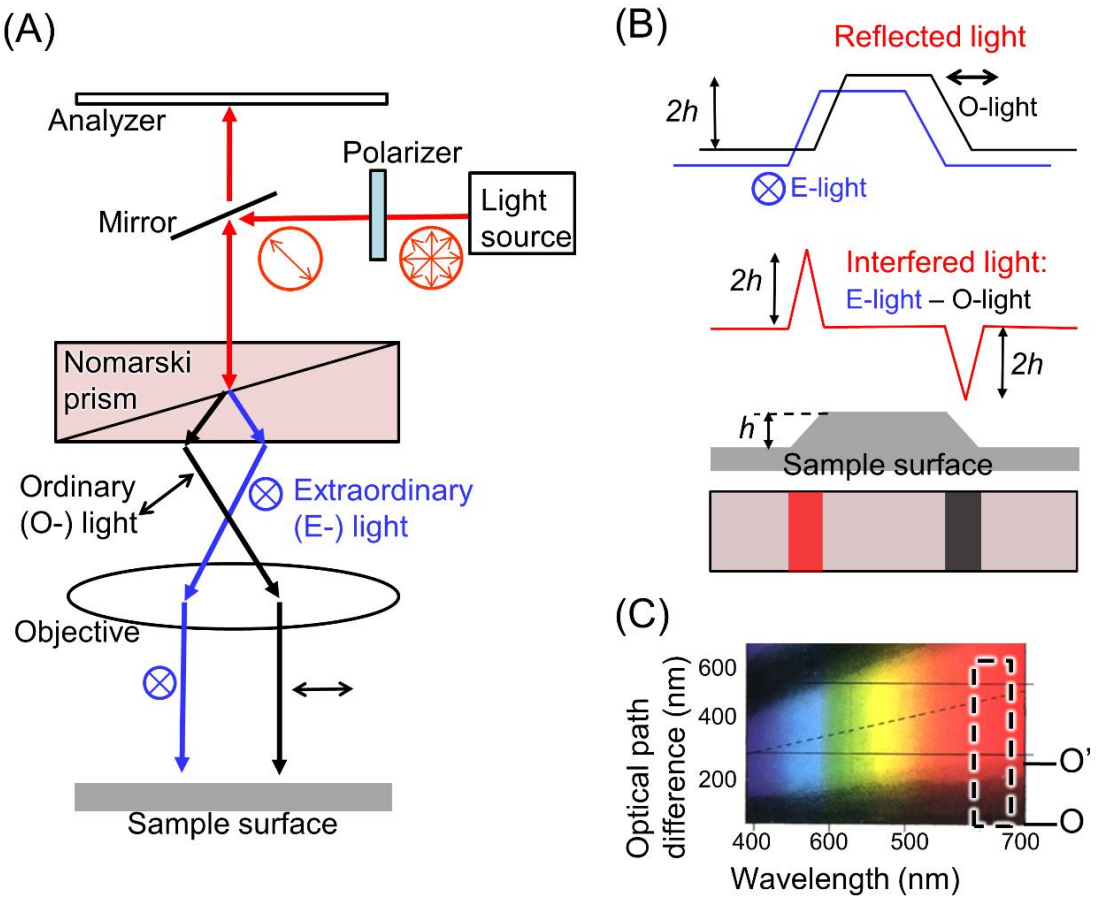

Fig. 2.2. A working principle of a reflection-type differential interference contrast microscope (DIM). (A) Path of the rays of the DIM. Using a Nomarski prism, a polarized light beam is separated into two parallel light beams, ordinary (O-) light (black) and extraordinary (E-) light (blue), with orthogonal vibrational directions. Then the two parallel light beams are reflected from a sample surface. (B) A cross-sectional schematic of a sample surface and changes in phases of reflected light and interfered light. When a sample surface has a height difference h, the two parallel light beams reflected from the sample surface have an optical path difference $2h$. When interference of the two light beams occurs at an analyzer, the E- and O-light beams are subtracted each other. (C) Relation between optical path difference and interference colors. A super luminescent diode (SLD) with a wavelength of 680 nm (red) was used. Therefore, with increasing optical path difference, the interference color changes from black to red, as indicated by a dotted rectangle. By intentionally adjusting the phase difference in the incident O- and E-light beams, the origin of the interference can be freely changed from a point O to a point O'.

2-1-3. An LCM-DIM and a Linnik interferometer

In order to study ice surfaces and quasi-liquid layers (QLLs) on ice surfaces, the LCM was combined with the DIM (LCM-DIM) and also with a Linnik interferometer, as shown in Fig. 2.3A. Two independent objectives of 20-fold magnification were equipped with the Linnik interferometer.

The LCM-DIM has advantages of both an LCM and a DIM. Noises originating from outside of a focal plane were excluded significantly by the LCM. In addition, three-dimensional contrast could be obtained by the DIM. Therefore, the LCM-DIM can give a three-dimensional contrast to subnanometer-height molecular steps on flat crystal surfaces[41].

However, because a laser beam has significantly better coherency than a white-light beam, unnecessary interferences, such as interference fringes and speckle patterns, are also obtained. Then to eliminate such unnecessary interferences, a super luminescent diode (SLD: Amonics Ltd., model ASLD68-050-B-FA), whose wavelength and coherent length were 680 nm and 10 μm, respectively, was used as a light source.

The DIM and the Linnik interferometer could be easily switched into each other. The Linnik interferometer was used to monitor the growth and sublimation of polycrystalline ice surfaces. Interference fringes could be formed by light beams reflected from an ice-vapor interface and a reference mirror. A compensator, which had the same thickness (0.45 mm) as that of a glass window of an observation chamber, was inserted into the interferometer. When a shutter was removed from or inserted into the Linnik interferometer, interference or bright-field images were obtained.

Because our confocal system was equipped with a polarization beam splitter [41], our optical microscope system worked as a reflection-type polarized light microscope whose directions of a polarizer and an analyzer were perpendicular each other.

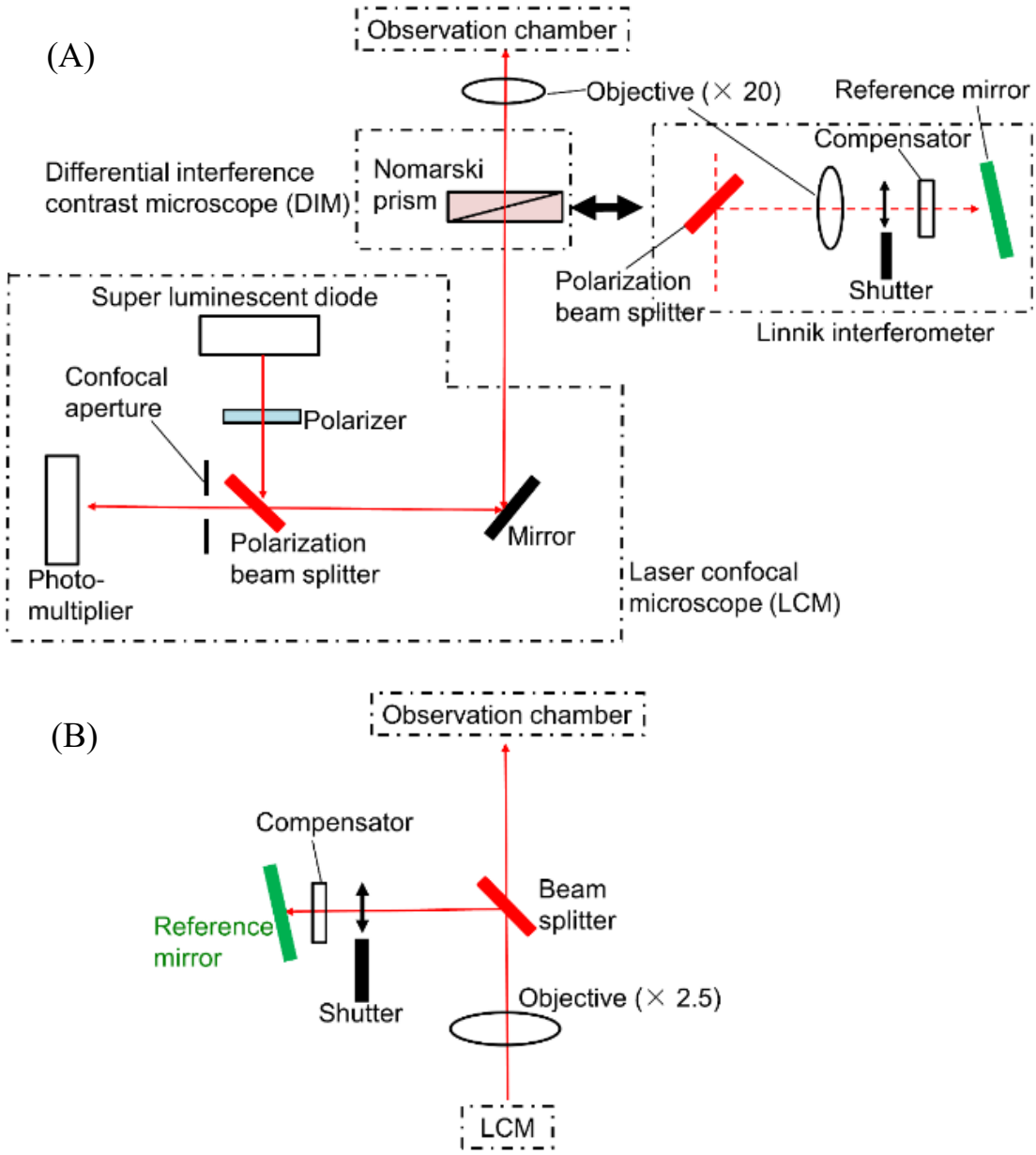

Fig. 2.3. A schematic drawing of our observation systems. A super luminescent diode was used as a light source. (A) The LCM was combined with the DIM and a Linnik interferometer. The DIM and the Linnik interferometer could be easily switched into each other easily. (B) A Michelson interferometer could also be equipped with the laser confocal system.

2-1-4. A Michelson interferometer

In addition, a Michelson interferometer whose magnification was 2.5-fold could also be equipped with the laser confocal system, as shown in Fig. 2.3B. Due to the thicker focal depth of the Michelson interferometer (170 μm) than that of Linnik interferometer (7.5 μm), more information from insides of ice grains could be obtained by using the Michelson interferometer [57].

2-2. An observation chamber

A home-made observation chamber was designed to observe polycrystalline ice thin films under certain temperature and water vapor pressure. Figure. 2.4 shows a cross-sectional schematic of the observation chamber, which was made of two copper (Cu) plates.

A polycrystalline ice thin film formed on a cover glass (the preparation of the polycrystalline ice thin film will be explained later in the section 2-3) was placed at the center of the upper Cu plate. On the lower Cu plate, ice crystals were also grown to supply water vapor to the polycrystalline ice thin film for the observation. The volume of the ice crystals on the lower Cu plate was significantly larger than that of the polycrystalline ice thin film. Through a triple-glasses window at the center of the lower Cu plate, the polycrystalline ice thin film could be observed from below.

Two thermistors had been carefully calibrated by using a standard thermistor (Takara Thermistor Co. LTD.) and a constant temperature water bath [58], before they were attached to the observation chamber. The temperatures of the upper and lower Cu plates were measured by the top and the bottom thermistors, respectively. The temperatures of the upper and lower Cu plates were separately controlled using Peltier elements, although the temperatures of Teflon blocks were not controlled actively.

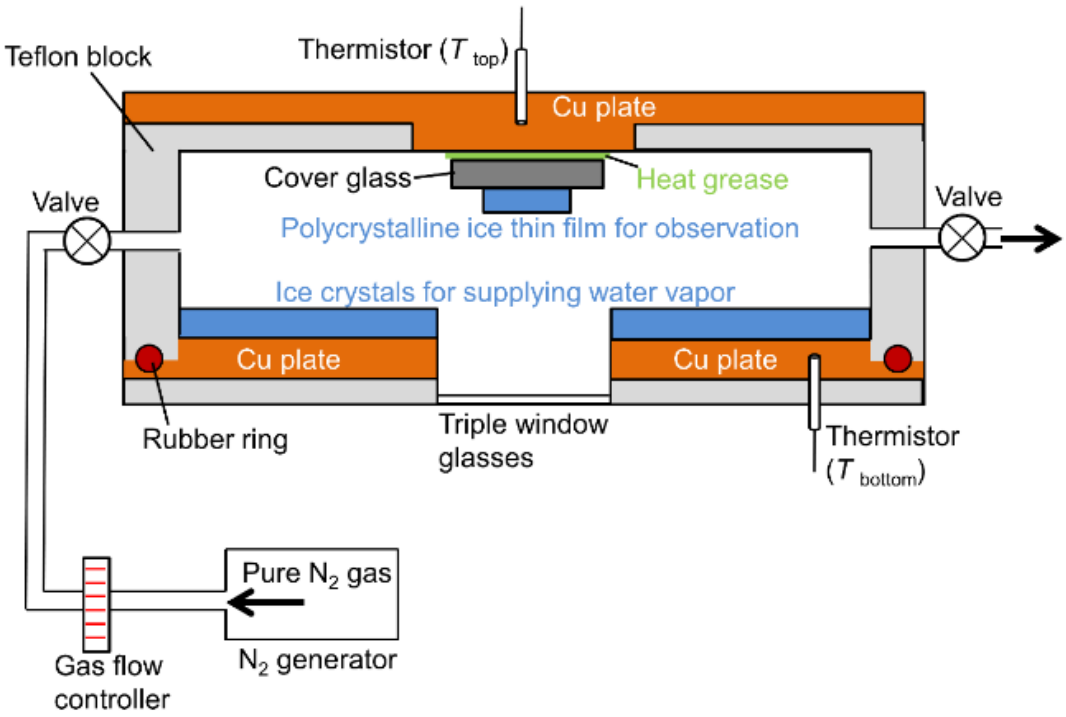

Fig. 2.4. A schematic drawing of an observation chamber. A cover glass, on which a polycrystalline ice thin film for observation was formed, was placed on an upper Cu plate, using heat grease. Ice crystals for supplying water vapor were grown on a lower Cu plate. Temperatures of the two Cu plate could be controlled separately. Pure N_2 gas could be injected into the observation chamber using a N_2 gas generator and a gas flow controller.

Two silicone tubes with valves were attached to the observation chamber to inject pure N_2 gas into the chamber. In addition, a rubber O-ring was sandwiched between the Teflon block and the lower Cu plate. When the valves were closed, the chamber bacame air-tight.

2-3. The preparation of polycrystalline ice thin films for observation

A polycrystalline ice thin film was prepared on a cover glass. As schematically shown in Fig. 2.5A, an aluminum block was located in a Styrofoam box and was cooled using liquid nitrogen (−196 °C). A round cover glass (12 mm in diameter) was placed

on the aluminum block. Ultrapure water (resistivity: 18 MΩ·cm) of ~5 μL was dropped on the cover glass from 1.2 m above using a syringe. The polycrystalline ice thin film thus formed on the cover glass had a diameter of 7−9 mm and a thickness of 70−80 μm, as shown in Fig. 2.5B. The polycrystalline ice thin film had a bump at its center, as shown in Fig. 2.5C. To obtain a homogeneous ice thin film, the ice thin film outside the bump was cut into a small piece (0.6× 0.6 mm^2), as shown in Fig. 2.5D. The other part of the ice thin film was removed from the cover glass. The preparation of the polycrystalline ice thin film of the small size was crucial in reducing the amount of water vapor necessary to grow the ice thin film and hence in decreasing the depletion of water vapor in the vicinity of the growing ice thin film [49]. Then the polycrystalline ice thin film for the observation on the cover glass was attached to the upper Cu plate of the observation chamber using heat grease (Fig. 2.4). After the drop of pure water on the cover glass, all processes were performed in a cold room at −10 °C.

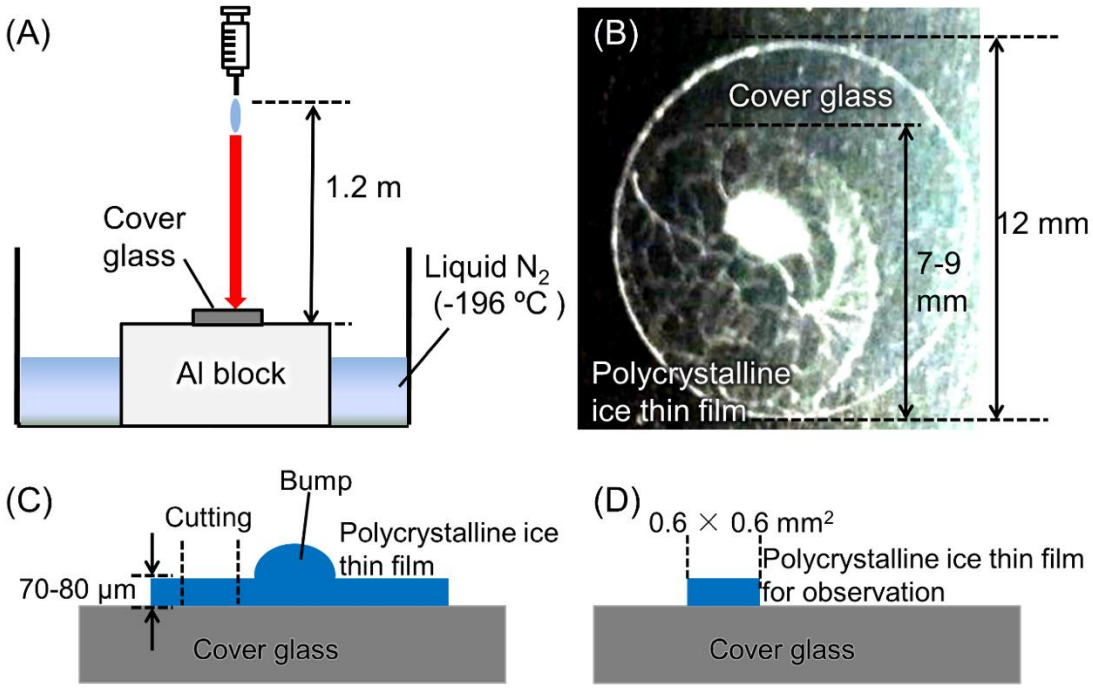

Fig. 2.5. The preparation of a polycrystalline ice thin film for observation. (A) A cover glass was placed on an Al block cooled by liquid N_2 (−196 °C). Ultrapure water (resistivity: 18 MΩ·cm) of ~5 μL was dropped on the cover glass with a diameter of 12 mm from 1.2 m above using a syringe. (B) By quenching the pure water, a polycrystalline ice thin film with a diameter of 7~9 mm was formed. (C) A cross-sectional schematic of the polycrystalline ice thin film. A bump was formed at the center of the ice thin film. (D) The polycrystalline ice thin film was cut into a small piece of 0.6× 0.6 mm^2 and the bump was removed away.

2-4. Calibration of temperature and water vapor pressure

Before the observation chamber was assembled, thermistors were calibrated carefully. However, thermal contact between the thermistors and the observation chamber could potentially have imperfection. In addition, the thermistors and the ice crystals were spatially separated. Hence, temperatures measured using the thermistors were different from the real temperatures of the polycrystalline ice thin films for the observation (T_{sample}) and the ice crystals for supplying water vapor (T_{source}). Therefore,

correct values of T_{sample} and T_{source} were obtained experimentally according to the recipes explained in the sections 2-4-1 and 2-4-2. Equilibrium water vapor pressure (P_e) of the polycrystalline ice thin films for the observation and water vapor pressure inside the observation chamber (P) were also determined using the correct values of T_{sample} and T_{source}. Hereafter, T_{top} and T_{bottom} show the temperatures of the upper and lower Cu plates, respectively, measured directly using the thermistors (corresponding to T_{sample} and T_{source} before the correction).

2-4-1. Calibration of T_{sample} and P_e

To obtain a correct value of T_{sample}, the temperature of the upper Cu plate, T_{top}, was corrected utilizing the melting temperature of the polycrystalline ice thin films (0 °C). Water vapor pressure P inside the chamber was kept slightly supersaturated throughout the calibration process by observing the growth of the polycrystalline ice thin films and also carefully adjusting the temperature T_{bottom}. Then as the temperature T_{top} was increased gradually, melting of the polycrystalline ice thin films was observed at $T_{top} = 0 + \delta$ °C. The value of δ ranged from +0.7 to +1.5 °C, depending on experimental runs. The real temperature of the polycrystalline ice thin films for the observation T_{sample} was obtained as

$$T_{sample} = T_{top} - \delta \text{ °C}. \quad \text{(E1)}$$

The value of P_e, which was determined by the evaporation of the polycrystalline ice thin films, was calculated from T_{sample} thus calibrated and the following ice-water vapor equilibrium curve or liquid water-water vapor equilibrium curve [59, 60]:

$$P_e(T) = \exp[29.33 - 6025 \cdot T_{sample}^{-1} + 1.061 \times 10^{-2} T_{sample} - 1.320 \times 10^{-5} T_{sample}^2 - 0.4940 \ln(T_{sample})] \quad (\text{when } T_{sample} \leq 273.2 \text{ K}), \text{ or}$$

$$P_e(T) = \exp[21.24 - 6097 \cdot T_{sample}^{-1} + 2.711 \times 10^{-2} T_{sample} - 1.674 \times 10^{-5} T_{sample}^2 + 2.433 \ln(T_{sample})] \quad (\text{when } T_{sample} > 273.2 \text{ K}). \quad \text{(E2)}$$

Here, the unit of T_{sample} is K (absolute temperature).

2-4-2. Calibration of T_{source} and P

Because of the structure of the observation chamber (Fig. 2.4), the ice crystals for supplying water vapor on the lower Cu plate could not be observed directly. Hence, at a certain constant T_{sample} (already calibrated in the section 2-4-1), T_{bottom} was increased and decreased. Then the growth and sublimation of the polycrystalline ice thin film for the observation were observed using the Linnik interferometer. From such interferometry observation, T_{bottom} at which the polycrystalline ice thin film was in equilibrium with water vapor pressure inside the chamber P (i.e. $P_e = P$) was determined as follows.

Figure 2.6A shows an example of an interference image observed on a polycrystalline ice thin film. Pixels along a dedicated line (X–Y in Fig. 2.6A were extracted from sequential images, and were stacked in a new x–y matrix. Figure 2.6B shows a spatiotemporal image, so called a time-space plot, when the distance between the ice surface and the interferometer was intentionally decreased using a stepper motor, at T_{sample}= −0.6 °C (already corrected) and T_{bottom} = −0.5 °C. The interference fringes were moved into the upper direction.

Figures 2.6C-D show time-space plots taken at a constant T_{sample}= −0.6 °C (already calibrated), and T_{bottom} = −0.5 °C and −0.6 °C, respectively: to take these two images the focus position was fixed. At T_{bottom} = −0.5 °C (Fig. 2.6C), the interference fringes were moved into the upper direction, showing the gradual decrease in the distance between the ice surface and the interferometer: i.e. the growth of the ice thin film. In contrast, at T_{bottom} = −0.6 °C (Fig. 2.6D), the interference fringes were moved into the lower direction, indicating the gradual increase in the distance between the ice surface and the interferometer: i.e. the sublimation of the ice thin film. From such interferometry observations, the value of T_{bottom} (= −0.55 °C), at which the growth rate of the polycrystalline ice thin film became approximately zero, could be determined. At such T_{bottom}, $P = P_e$. Hence, the real temperature of the ice crystals for supplying water vapor $T_{source} = T_{sample}$ (already calibrated).

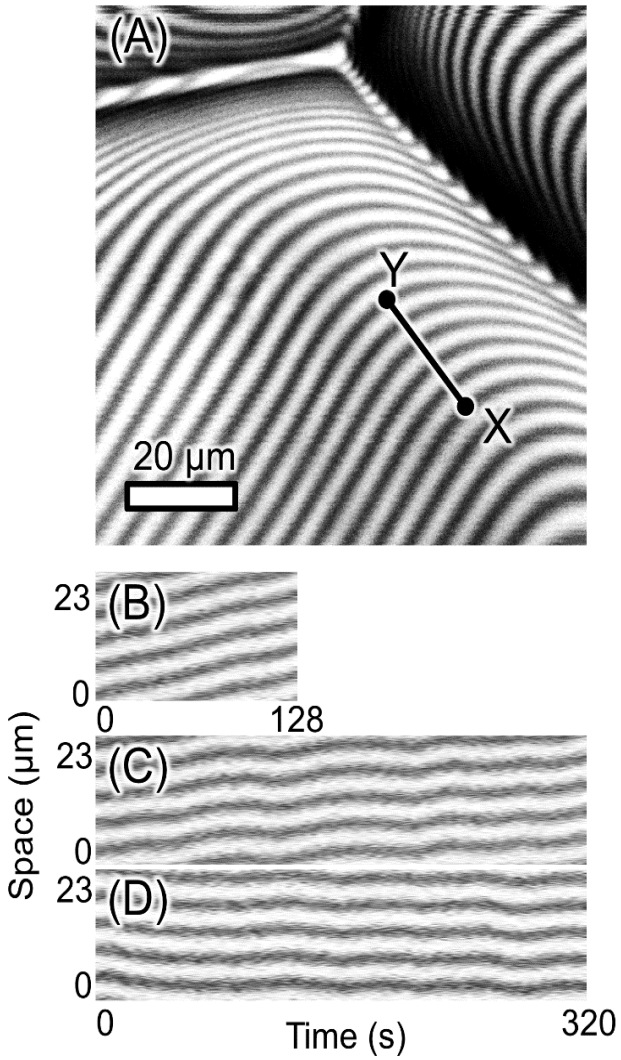

Fig. 2.6. Interferometry observations at a constant sample temperature T_{sample} = −0.6 °C (already calibrated). (A) A polycrystalline ice thin film observed using the Linnik interferometer at T_{bottom} = −0.5 °C. A dedicated line *X*-*Y* was used for preparing time-space plots showing movement directions of interference fringes to judge whether the polycrystalline ice thin film was under a supersaturated or undersaturated condition. (B) A time-space plot showing the movement of interference fringes when the distance between the ice surface and the interferometer was intentionally decreased using a stepper motor, at T_{bottom} = −0.5 °C. (C and D) Time-space plots taken at T_{bottom} = −0.5 and −0.6 °C, respectively: to take the interferometry images, the focus position was fixed.

Under various constant T_{sample}, similar measurements were performed. Figure. 2.7 shows the relation between T_{bottom} and T_{source} when $P = P_e$. The linear relation shown in Fig. 2.7 is

$$T_{source} = 0.9514 \cdot T_{bottom} - 0.0060. \quad \text{(E3)}$$

Here, the unit of T is °C. From equation (E3), correct values of T_{source} (= T_{sample}) were obtained under various T_{bottom}. Finally, from the correct value of T_{source} thus obtained and equation (E2), P, which was determined by the evaporation of the ice crystals for supplying water vapor, could be calculated correctly. After each observation experiment was finished, all above-mentioned processes were performed to correctly determine T_{sample}, T_{source}, P_e and P.

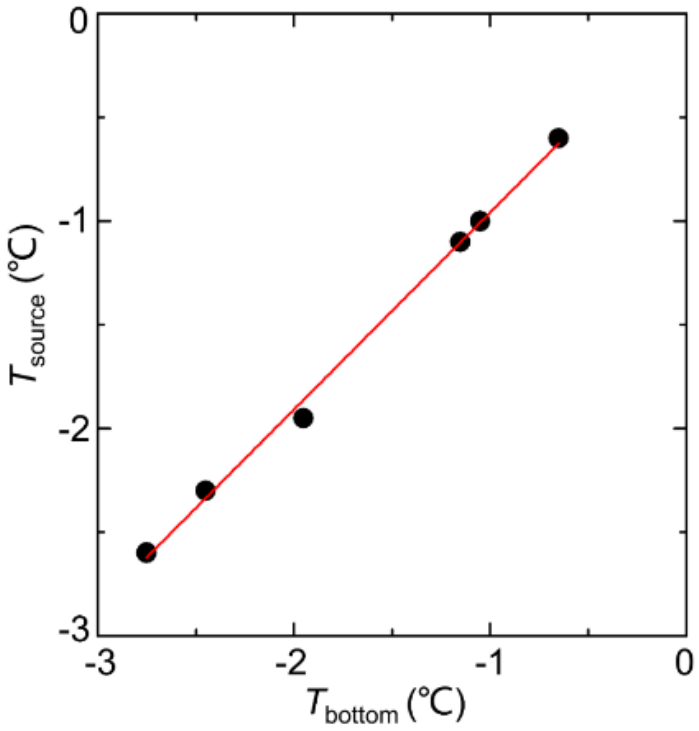

Fig. 2.7. The relation between a measured temperature of a bottom Cu plate (T_{bottom}) and a real temperature of ice crystals for supplying water vapor (T_{source}). The red line shows the result of linear fitting. Black dots present values obtained by calibration experiments.

If elementary steps on the polycrystalline ice thin film could be observed by LCM-DIM, the accuracy of the determination of T_{bottom} and P was very high. However, the

surface of the polycrystalline thin film was curved macroscopically (i.e. rough at the molecular size scale), disabling the visualization of elementary steps. Therefore, to maintain the accuracy, the vapor-ice equilibrium was determined from the time-space plots taken for longer than 5 mins (Figs. 2.6C and D).

2-4-3. Experimental errors

The error of the determination of T_{source} was ±0.05 °C: this value was calculated from the standard deviation of the data shown in Fig. 2.7. From the propagation of error, the error of the water vapor pressures P and P_e was estimated at ±2 Pa. Hence, the supersaturation of water vapor, $\sigma = P/P_e$, exhibited the error of ±0.004.

2-5. Cleaning a surface of a polycrystalline ice thin film

All the processes mentioned in the section 2-3 were performed in room air. Hence, the ice surface was inevitably exposed to air, and the chamber was fulfilled with air. To avoid possible bias caused by atmospheric reactive gasses, and to obtain fresh (uncontaminated) surfaces of the polycrystalline ice thin films, pure N_2 gas was injected into the chamber.

After the observation chamber was placed on the optical microscope, T_{sample} and P were set at $T_{sample} = -9$ °C and $P = 285$ Pa ($P_e = 284$ Pa), to keep polycrystalline ice thin films under slightly supersaturated water vapor. Then pure N_2 gas was injected into the chamber at a constant rate of 0.4 L/min for more than 10 min. Because the inner volume of the chamber was ~5 mL, the air in the observation chamber was fully replaced with pure N_2 gas at atmospheric pressure.

During the injection of the N_2 gas, the surface of the polycrystalline ice thin film was sublimated. To monitor the amount of sublimation, the polycrystalline ice thin film was observed using the Linnik interferometer. The interference fringes were moved into one direction. The decrease in the thickness of the polycrystalline ice thin film, ΔH,

was calculated by

$$\Delta H = \frac{L}{l} \cdot \frac{\lambda}{2} .$$

Here, L is the length of the movement of one interference fringe; λ is the wavelength of the light source (680 nm); l is the distance between adjacent interference fringes. During the injection of the N_2 gas, the polycrystalline ice surface was sublimated by 3~4 μm in thickness. After the injection of the N_2 gas, the observation chamber was kept airtight, and then the polycrystalline ice thin film was used for further observation.

3. Characters of polycrystalline ice thin films

In this chapter, we show behaviors of ice grains in polycrystalline ice thin films observed by our optical microscopes. We discuss crystallographic orientations of polycrystalline ice grains in the section 3-1 and rate of grain growth in the section 3-2.

3-1. Orientations of polycrystalline ice grains

In order to characterize crystallographic orientations of ice grains in polycrystalline ice thin films, we need to obtain information from insides of the ice grains. Therefore, we used a polarized-light optical microscope of a reflection type, equipped with an objective lens which had a thick focus depth (a small magnification). In this section, we used a Michelson interferometer (4× magnification) whose focus depth is about 170 μm (see Appendix B), after we inserted a shutter in the optical path of a reference mirror (Fig. 2.3B) to prohibit light from reflecting at the reference mirror and to obtain a bright-field image.

Fig. 3.1 shows a bright-field image of a polycrystalline ice thin film at a T_{sample} = −9.5 °C (P_{e} = 272 Pa) and P = 295 Pa, taken using the reflection-type polarized light optical microscope. We could find that all ice grains of the polycrystalline ice thin film show various contrasts. Note that the ice grains marked by black, white, and black-white arrowheads show dark, white, and grey (intermediate) contrasts, respectively.

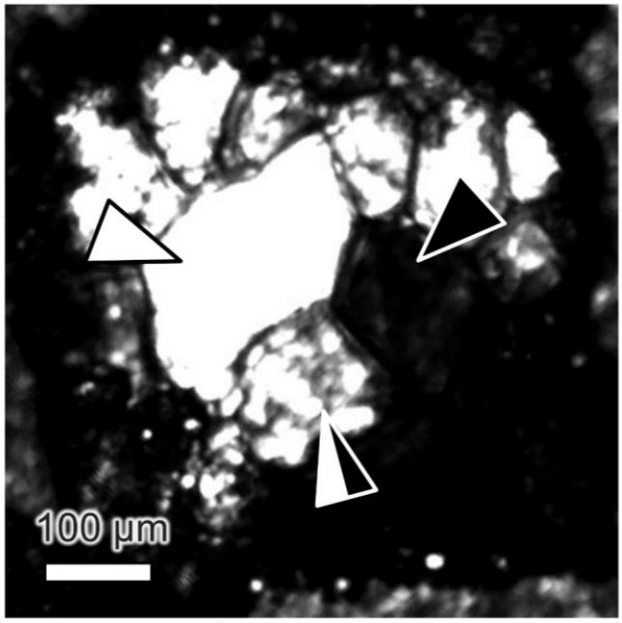

Fig. 3.1. A bright-filed image of a polycrystalline ice thin film observed using a polarized-light microscope of a reflection type, at T_{sample} = −9.5 °C (P_e = 272 Pa) and P = 295 Pa. To obtain such an image, a shutter was inserted in an optical path of a reference mirror of a Michelson interferometer (2.5-fold magnification). The black, white and white-black arrowheads indicate ice grains shown in dark, white, and grey contrasts, respectively.

Our optical microscopy system could work as the reflection-type polarized light microscope whose directions of a polarizer and an analyzer were perpendicular to each other. When we observed the polycrystalline ice thin film using this microscopy system, a significantly large amount of polarized light was reflected from the insides of the ice grains due to the thick focus depth of 170 μm. Therefore, the various contrasts of the grains (Fig. 3.1) demonstrate that the crystallographic orientations of the grains varied substantially, as explained below:

When a polarized light was reflected from an optically isotropic grain, whose c-axis was almost parallel to the optical axis, a polarization plane of a light beam reflected from the grain was not rotated. Hence such the reflected light beam could not be transmitted through a polarization beam splitter (an analyzer) in our observation system (Fig. 2.3). Therefore, the optically isotropic ice grains whose c-axes were

almost parallel to the optical axis exhibited a darker contrast (shown by a black arrowhead in Fig. 3.1) than other grains.

In contrast, when a polarized light was reflected from an optically anisotropic grain, a polarization plane of a reflected light beam was rotated and then transmitted through the polarization beam splitter (the analyzer) (Fig. 2.3). Then such a grain could exhibit a brighter (grey or white) contrast than others, (indicated by the white and the black-white arrowheads respectively in Fig. 3.1), depending on the amount of anisotropy of the ice grain. Hence, the various contrasts observed on the ice grains demonstrate that the ice grains were randomly oriented in the polycrystalline ice thin films.

3-2. Grain growth of polycrystalline ice grains

We next observed grain growth of a polycrystalline ice thin film using the LCM-DIM. Figure 3.2A presents an LCM-DIM image of a polycrystalline ice thin film at T_{sample}=−2.1 °C and P=534 Pa (P_e =514 Pa). Figure. 3.2B was taken 38 min after the image shown in Fig. 3.2A. Figures. 3.2C1-C4 present time course of LCM-DIM images in the area marked by the dotted rectangle in Fig. 3.2A. As indicated by black arrows, some grains exhibited relatively fast grain growth, whose time scale was about 30 min at T_{sample} =−2.1 °C. In contrast, a comparison between Fig. 3.2A and B shows that some other grains (marked by black arrowheads in Fig. 3.2B) exhibited relatively slow grain growth. Such substantial variation in the speed of the grain growth is probably due to the variation in the characteristics of the grain boundaries. The relation between the characteristics of grain boundaries and misorientation of grains has been understood [61-63], and pioneering works on grain boundaries in ice crystals have also been reported [64-66].

We performed similar observations at various T and P. The average lateral size of grains was 170±75 μm. To eliminate the effects of the grain growth, we excluded grains that exhibited the relatively fast grain growth (within ~30 min) from further examinations of the appearance of QLLs.

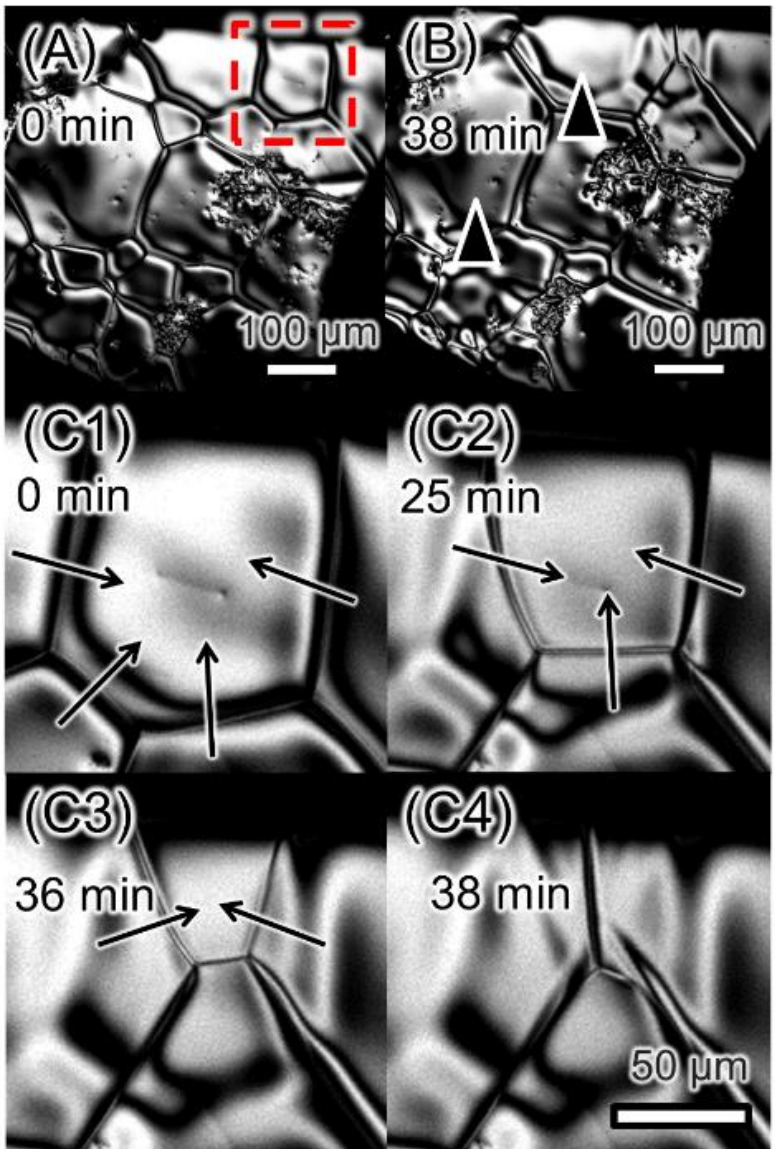

Fig. 3.2. A polycrystalline ice thin film and its behavior of grain growth at T_{sample}= −2.1 °C and P=534 Pa (P_e=514 Pa). (A) An LCM-DIM image of the polycrystalline ice thin film. (B) An LCM-DIM image taken 38 min after (A). Black arrowheads indicate grains showing relatively slow grain growth. (C1-C4) Time course of LCM-DIM images in the area marked by the dotted rectangle in (A). An image (C1) corresponds to a part of the image (A). The time in the images C2-C4 presents the elapsed time after the image (C1) was taken. Black arrows indicate grain boundaries exhibiting relatively fast grain growth and their directions of movement. An image (C4) corresponds to a part of the image (B).

4. Quasi-liquid layers (QLLs) in grooves of grain boundaries and on grain surfaces

In this chapter we show formation processes of quasi-liquid layers (QLLs) in grooves of grain boundaries and on grain surfaces of polycrystalline ice thin films, in a temperature range of −2.6 to −0.4 °C. First we prove the existence of QLLs in grooves of grain boundaries in the section 4-1. Then we show the experimental results of QLLs on grain surfaces in the section 4-2. Next we explain the temperature range in which QLLs can be formed, and discuss the formation mechanisms of the QLLs in the section 4-3. Finally, we summarize the results in the section 4-4.

4-1. QLLs in grooves of grain boundaries

Direct observation of QLLs formed in grooves of grain boundaries is extremely difficult because of the minute thickness (1-10 nm) of grain boundaries [67, 68]. Therefore, in order to prove the existence of QLLs formed in grooves of the grain boundaries, we added polystyrene particles (653 nm in diameter and 0.02% in volume fraction) into pure water, when we prepared polycrystalline ice thin films. Then we tried to observe movement of the polystyrene particles after volume of QLLs became large enough to move the particles.

Figure. 4.1 shows a phase diagram of ice (water), and indicates changes in temperatures during experiments performed in this section. The pressure-temperature regions (shown in blue and red colors in the supersaturated and undersaturated conditions, respectively) in which QLLs exist kinetically (and also continuously) on surfaces of ice single crystals [46, 47]. Black arrows indicate temperature changes (at constant water vapor pressure) that we performed in Figs. 4.2 and 4.3. As shown in Fig. 4.1, in the vicinity of the vapor-ice and vapor-liquid water equilibrium curves (solid and dotted curves), QLLs cannot exist kinetically on ice single crystals.

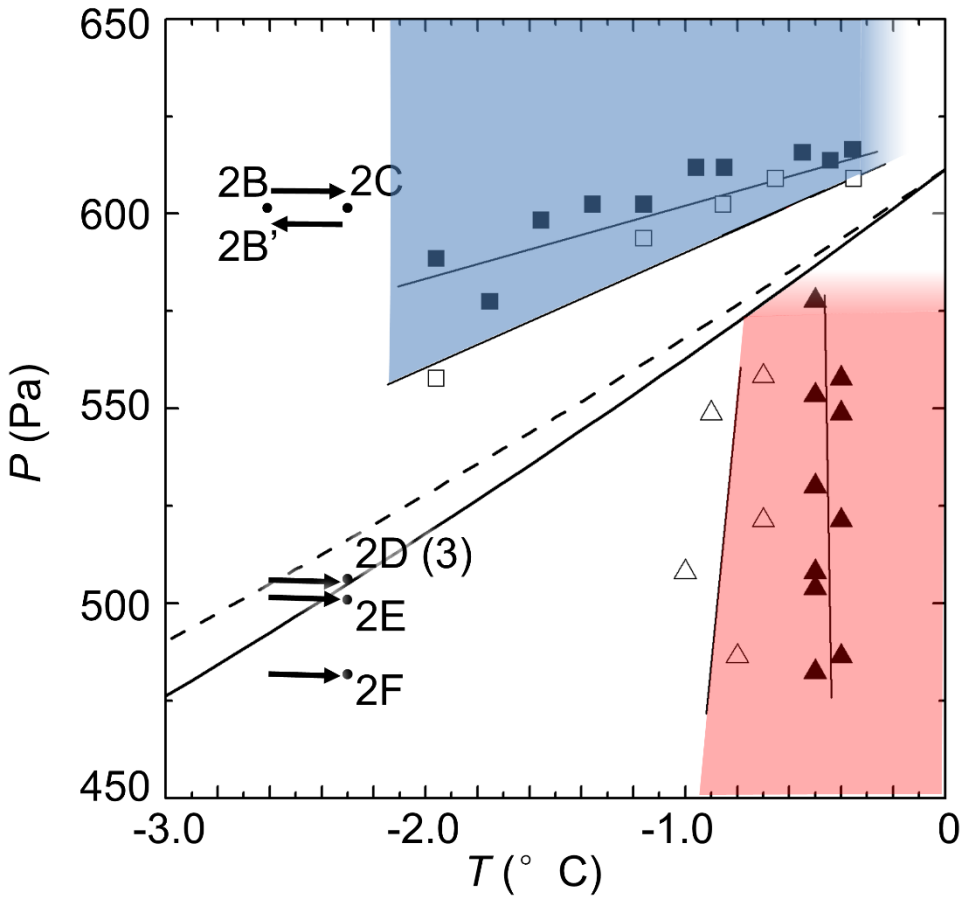

Fig. 4.1. Experimental conditions of the observations shown in Figs. 4.2 and 4.3, and a pressure-temperature (*P*-*T*) phase diagram for water and the *P*-*T* regions in which QLLs exist kinetically and continuously on ice single crystals [46, 47]. Black arrows indicate the temperature changes (at various constant pressures), and number-letter combinations beside the arrows correspond to figure numbers in Figs. 4.2 and 4.3. On surfaces of ice single crystals, open squares (triangles) indicate critical water vapor pressures (temperatures) above which droplet-type QLLs exist kinetically; solid squares (triangles) indicate critical water vapor pressures (temperatures) above which thin-layer-type QLLs exist kinetically. Solid and dotted curves represent the vapor-ice and vapor-liquid water equilibrium curves, respectively. The rightmost and uppermost portions of the blue- and red-colored regions are shown by gradations in colors, respectively, indicating a lack of experimental datum. Hence the existence of QLLs is not indicated in these regions.

4-1-1. Motion of polystyrene particles in grooves of grain boundaries

In Fig. 4.2A, white arrowheads show polystyrene particles located in a groove of a grain boundary and on a grain surface. Here, we observed the mixture of the differential interference contrast and a part of light scattered from the particles. Figure 4.2B shows time course of LCM-DIM images of a polystyrene particle located in a grain boundary marked by the dotted rectangle in Fig. 4.2A at T_{sample} = −2.6 °C (P_e = 492 Pa) and P = 602 Pa. At −2.6 °C we could observe no movement of the particle in the groove.

In contrast, with increasing temperature from −2.6 °C to −2.3 °C (P_e = 505 Pa) at the constant pressure of 602 Pa, the particle moved in one direction along the groove of the grain boundary, as shown in Fig. 4.2C. After we took the images in Fig. 4.2C, we decreased temperature to −2.6 °C again (at the constant pressure) and took the images. Figure. 4.2B' indicates that the particle position was fixed again as observed in Fig. 4.2B. The change in temperature from −2.6 to −2.3 °C (and also that from −2.3 to −2.6 °C) was completed within 1 min. In these images, a time of 0 s shows the moment when the temperature became constant after the temperature change. We repeated similar observations changing temperature, and found that the starting and stopping of the particle movement of the particle in the same groove were highly reproducible.

We performed similar observations by increasing the temperature from −2.6 to −2.3 °C under different water vapor pressures at 506 Pa (Fig. 4.2D), 501 Pa (Fig. 4.2E), and 482 Pa (Fig. 4.2F). Figures 4.2D, E and F clearly demonstrate that irrespective of the water vapor pressure, the particle moved along the groove of the grain boundary at −2.3 °C, indicating that liquid water whose volumes were sufficient to move the particle existed in the groove at these water vapor pressures. We also found that in the grooves of grain boundaries, polystyrene particles continuously moved for even more than five hours when P and T_{sample} were constant. The particles did not stop moving in the grooves after once the particles started to move.

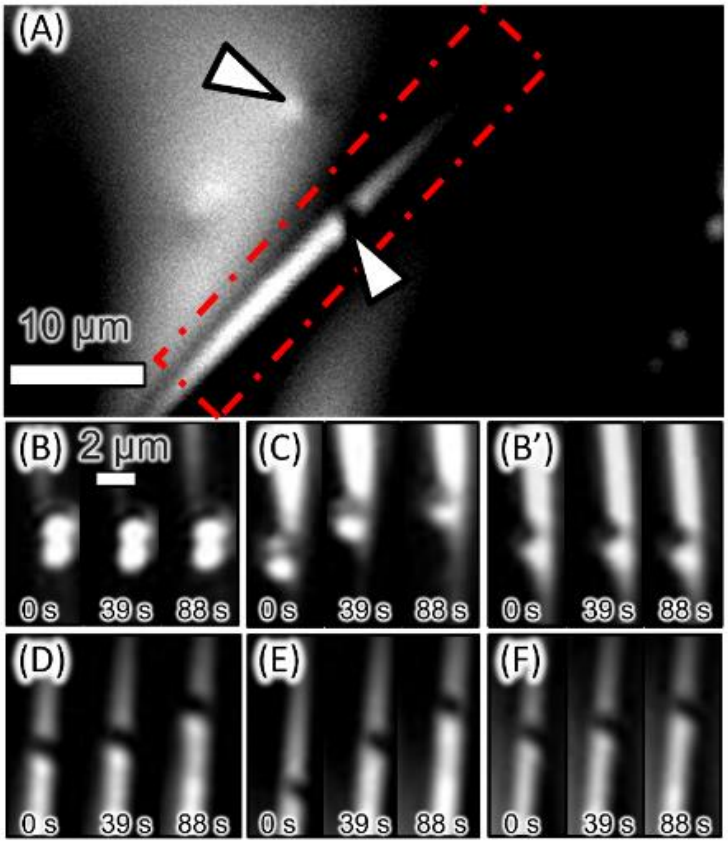

Fig. 4.2. The movement of a polystyrene particle in a groove of a grain boundary of a polycrystalline ice thin film. (A) An LCM-DIM image of the polycrystalline ice thin film at T_{sample}= −2.6 °C (P_e=492 Pa) and P=506 Pa. White arrowheads show polystyrene particles located in the groove of the grain boundary and on the grain surface. (B to F) Time course of LCM-DIM images in the area marked by the dotted rectangle in the image A: (B and B') T= −2.6 °C and P=602 P, (C) T= −2.3 °C (P_e=505 Pa) and P=602 Pa, (D) T= −2.3 °C and P=506 Pa, (E) T= −2.3 °C and P=501 Pa, and (F) T= −2.3 °C and P=482 Pa. The change in temperature from −2.6 to −2.3 °C (and also from −2.3 to −2.6 °C) occurred less than 1 min. In images B-F, a time of 0 s corresponds to the moment at which the temperature became constant after the temperature change. In the images B and B', the polystyrene particles in the groove were fixed. In contrast, in the images C, D, E and F, the polystyrene particles were moved along the groove as time elapsed.

In addition, it is also noteworthy that the particle located on the grain surface (Fig. 4.2A) never changed its position during the observation of T_{sample} increasing to −2.3 °C at P = 505 Pa, as shown in Fig. 4.3. This result clearly demonstrates that there exists no liquid water on the grain surface.

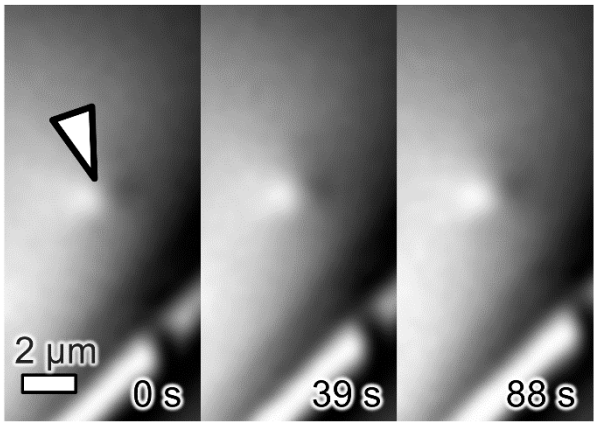

Fig. 4.3. A polystyrene particle located on a grain surface at T_{sample}= −2.3 °C (P_e=505 Pa) and P=606 Pa. T_{sample} and P were the same as those in Fig. 4.2D. The particle was the same as that shown in Fig. 4.2A. Irrespective of elapsed time, the polystyrene particle indicated by a white arrowhead was fixed at the same position.

4-1-2. Formation of QLLs in grooves of grain boundaries

At temperatures higher than −4 °C, grain growth and thermal roughening occurred [44]. Hence the deformation of grains during such processes could also change the positions of the polystyrene particles in the grooves. However, as shown in the section 3-1, even the relatively fast grain growth at −2.1 °C proceeded on the time scale of 30 min. In this temperature range, thermal roughening also occurred over 15 min to 7 h [44]. In contrast, we could observe the significant movements of the particles within 100 s (Figs. 4.2C, D, E and F). Hence, from the significant difference in the time scales, we concluded that the movements of the particles indicate the appearance of liquid water whose volume was sufficient to move the particles. In other words, the immobile

particles in the grooves (Figs. 4.2B and B') demonstrated that no liquid water existed in the grooves of the grain boundaries or that the volume of liquid water was insufficient to move the particles. Here, note that the absence of the movement of the particles at −2.6 °C was not due to the increase in the viscosity of the liquid water, because the viscosity of supercooled water at 0 and −2.6 °C is 1.8 and 2.0 (mPa·s) [69], respectively: the increase in the viscosity was moderate.

Can the liquid water that appeared in the grooves of the grain boundaries be considered a QLL? The movement of the polystyrene particles of 653 nm in diameter shows that the thickness of the liquid water in the grooves of the grain boundaries was comparable to the size of the particles. However, in our previous studies, the thickness of droplet-type QLLs that appeared on basal faces ranged from several tens of nanometers to 1 μm [42, 46]. Nevertheless the droplet-type QLLs exhibited a viscosity 20 times higher than bulk water [43]. Hence, the thickness of the liquid water in the grooves was also comparable with that of the QLLs on basal faces. In addition, if "real bulk water" exists on ice crystal surfaces, the bulk water can exist only for very short time period, because the normal growth of ice crystals in bulk melt is extremely fast (10^{-2} -10^{-7} m/s) [70, 71]. Hence, we concluded that the liquid water that appeared in the grooves of the grain boundaries was a QLL.

In Figs. 4.2C-F, the particles did not show random (Brownian) motion but showed the unidirectional motion. On basal and prism faces of ice single crystals, such unidirectional motions of droplet-type and thin-layer-type QLLs are often observed [42]. The unidirectional motion is probably due to the non-uniformity in temperature and water vapor pressure [72], although the actual reason is still unclear.

As shown in Fig. 4.1, QLLs can only exist kinetically in relatively higher supersaturated conditions (blue region) or relatively lower undersaturated conditions (red region) on surfaces of ice single crystals. And QLLs cannot exist kinetically in the vicinity of the vapor-ice and vapor-liquid water equilibrium curves. However, in this study, we found that QLLs, whose volumes were sufficient to move the particles, could be formed in grooves of grain boundaries irrespective of water vapor pressure, even in the immediate vicinity of the vapor-ice equilibrium curve (the points 2D and 2E in Fig.

4.1). This result clearly indicates that the QLLs in the grooves were mainly supplied by the grain boundaries, not by deposition of supersaturated water vapor or sublimation of ice as the cases on ice single crystals [46, 47].

4-1-3. Formation of QLLs in grooves of different grain boundaries

We performed similar observations, using polystyrene particles located in grooves of different grain boundaries. We found that the temperature at which polystyrene particles started to be moved by QLLs shows a significant variation.

Figure. 4.4A shows an example of a polycrystalline ice thin film at −2 °C (P_e= 518 Pa) and 560 Pa, taken using the LCM-DIM. We could see polystyrene particles indicated by white arrowheads were located in grooves of grain boundaries.

Figure 4.4B shows an enlarged image of the area marked by a dash-dotted rectangle in Fig. 4.4A. As marked by white arrowheads, a polystyrene particle in a groove of a grain boundary was moved along the groove as time elapsed. However, a polystyrene particle located in a groove shown in the area marked by a dotted rectangle in Fig. 4.4A exhibited different behavior. As shown in Fig. 4.4C, the particle was fixed at the same position, irrespective of elapsed time.

The difference in the critical temperature, above which QLLs can appear in grooves of grain boundaries, was probably caused by the difference in the properties of the grain boundaries. As shown in the section 3-1, all ice grains in the polycrystalline ice thin films used in this study were randomly orientated. Hence the characters of grain boundaries vary depending on the crystallographic orientations of adjacent ice grains.

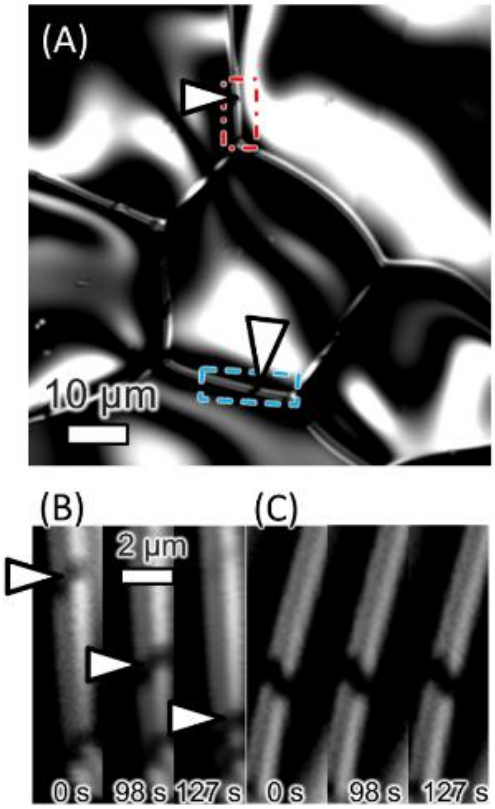

Fig. 4.4. Behaviors of polystyrene particles in grooves of different grain boundaries. (A) A polycrystalline ice this film with polystyrene particles in grooves of grain boundaries at T_{sample}= −2 °C (P_e= 518 Pa) and 560 Pa. (B) An enlarged picture of the area marked by the red dash-dotted rectangle in the image A. A polystyrene particle indicated by a white arrowhead was moved as time elapsed. (C) An enlarged and clock-wise rotated picture of the area marked by the blue dotted rectangle in the image A. A polystyrene particle in a groove of a grain boundary was fixed at the same position.

4-2. QLLs on grain surfaces

4-2-1. Droplet-type QLLs

We further increased the temperature and observed ice grain surfaces. Figure. 4.5 shows a phase diagram of ice (water) and experimental conditions in this section. Red arrows indicate the temperature changes (at constant water vapor pressure) that we performed in Figs. 4.6 and 4.7.

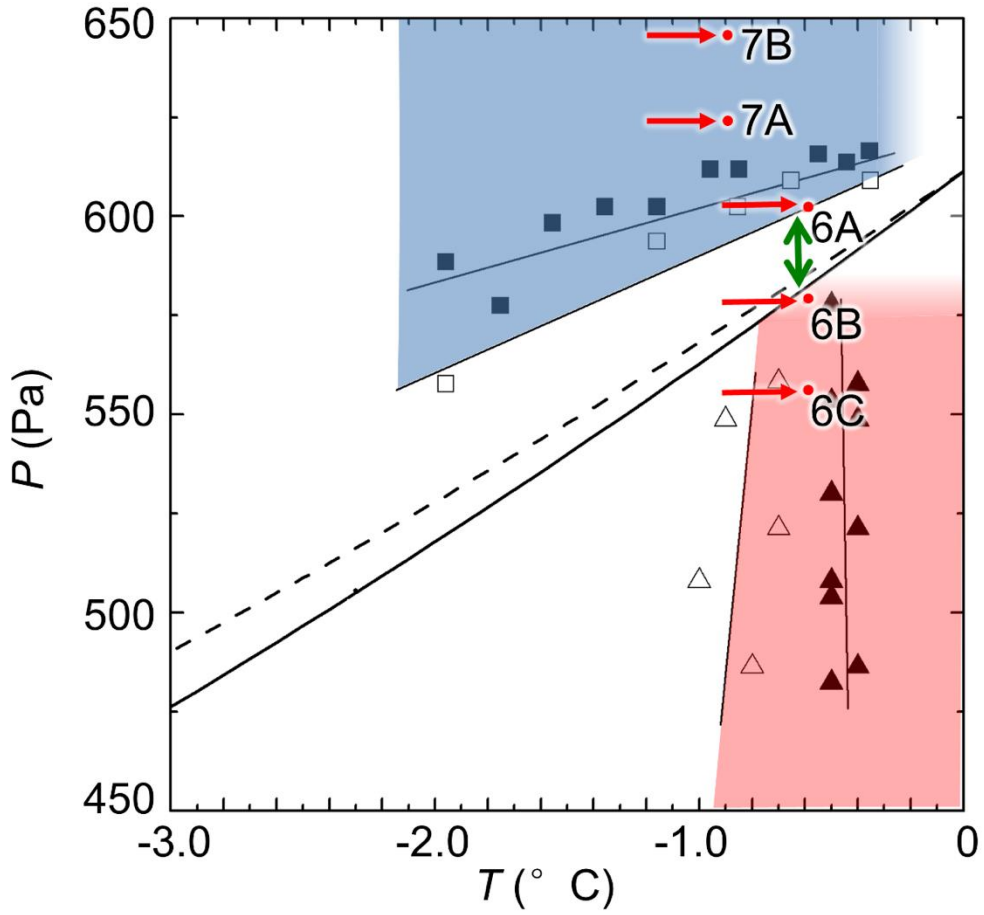

Fig. 4.5 Experimental conditions of the observations shown in Figs. 4.7 and 4.8, and a pressure-temperature (*P*-*T*) phase diagram for water and the *P*-*T* regions in which QLLs exist kinetically and continuously on ice single crystals [46, 47]. Red arrows indicate the temperature changes (at various constant pressures), and number-letter combinations beside the arrows correspond to figure numbers in Figs. 4.6 and 4.7. A pressure-temperature (*P*-*T*) phase diagram for water and the *P*-*T* regions in which QLLs exist kinetically and continuously on ice single crystals [46, 47]. On surfaces of ice single crystals, open squares (triangles) indicate critical water vapor pressures (temperatures) above which droplet-type QLLs exist kinetically; solid squares (triangles) indicate critical water vapor pressures (temperatures) above which thin-layer-type QLLs exist kinetically. Solid and dotted curves represent the vapor-ice and vapor-liquid water equilibrium curves, respectively. The rightmost and uppermost portions of the blue- and red-colored regions are shown by gradations in colors, respectively, indicating a lack of experimental datum. Hence the existence of QLLs is not indicated in these regions.

We show a typical example in Fig. 4.6, when we raised temperature from −0.9 to −0.6 °C (P_e= 582 Pa) under various water vapor pressure. Figure. 4.6A presents time course of LCM-DIM images under supersaturated water vapor (P= 602 Pa and P_e= 582 Pa). After we raised temperature from −0.9 to −0.6 °C, droplet-type QLLs appeared on the grain surface within a couple of minutes, as on basal faces of ice single crystals [42]. In this study, the differential interference contrast was adjusted as if the sample surface was illuminated by a light beam slanted from the lower-left to the upper-right direction. Hence, the lower-left and upper-right halves of the droplet-type QLLs appeared bright and dark, respectively. White lines shown in the lower-left corner of the field of view indicate a groove of a grain boundary between adjacent grains.

Figure. 4.6' shows time course of LCM-DIM images in the area marked by the dotted rectangle in Fig. 4.6A (at 185 s). As time elapsed, adjacent droplet-type QLLs coalesced with each other at the positions marked by black arrows. This result clearly demonstrates that the droplet-type QLLs appearing on the grain surface exhibited macroscopic fluidity, and that they were not solid but liquid formed on the grain surface at temperature below 0 °C. Hence they should be called as QLLs.

In Fig. 4.6A, however the droplet-type QLLs reached their maximum size (185 s) and then spontaneously disappeared (736 s), although the temperature and water vapor pressure were kept constant. We could not find such spontaneous disappearance of the droplet-type QLLs on surfaces of ice single crystals in the blue and red P-T range in Fig. 4.5.

In addition, we performed similar observations to study the effects of water vapor pressure. Figures. 4.6B and C also show time course of LCM-DIM images taken in the immediate vicinity of the vapor-ice equilibrium curve (P= 578 Pa and P_e= 582 Pa) and under highly-undersaturated water vapor condition (P= 556 Pa and P_e= 582 Pa), respectively. As shown in Figs. 4.6B and C, even under these water vapor pressures, after we raised temperature from −0.9 to −0.6 °C, drop-type QLLs appeared on the grain surface within a couple of minutes, and then spontaneously disappeared within 10 min.

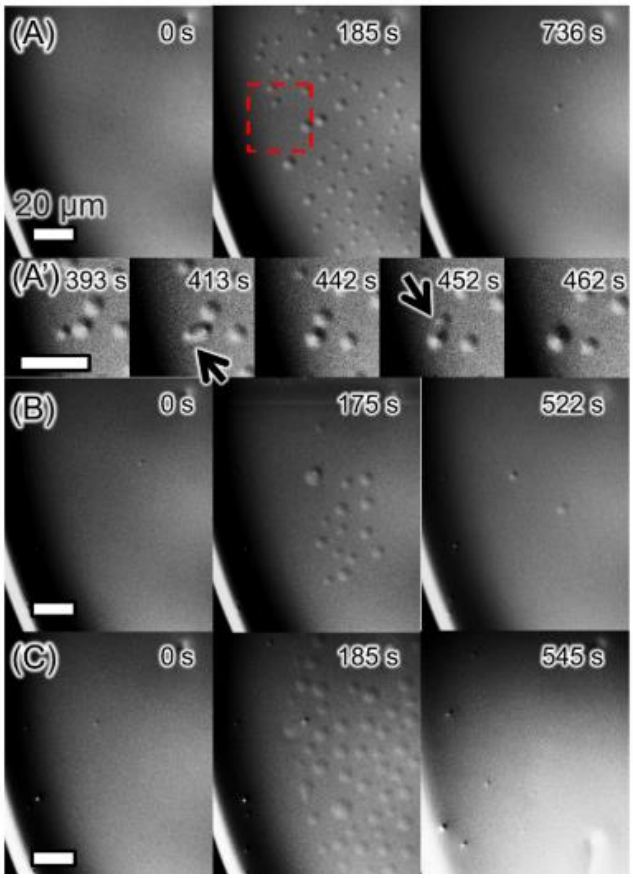

Fig. 4.6. The emergence and subsequent disappearance of droplet-type QLLs on surfaces of ice grains at −0.6 °C (P_e=582 Pa). Time course of LCM-DIM images of the grain surfaces were taken at (A) P=602 Pa, (B) P=578 Pa, and (C) P=556 Pa. These P-T conditions correspond to the points 6A-6C in Fig. 4.6. After the temperature was raised from −0.9 °C to −0.6 °C, the droplet-type QLLs appeared on the grain surface within a couple of minutes, but subsequently disappeared gradually from the grain surface as additional time elapsed. The temperature increase from −0.9 to −0.6 °C occurred within 1 min. In images A-C, the time of 0 s corresponds to the moment at which temperature was started to increase. Images A' also show detailed time course of enlarged LCM-DIM images in the area marked by the dotted rectangle in the image A (at 185 s) during the process A. Adjacent droplet-type QLLs coalesced with each other at the positions marked by black arrows, clearly demonstrating macroscopic fluidity of the droplet- type QLLs. All scale bars correspond to 20 μm.

To reveal whether QLLs could stably exist at a relatively higher supersaturated condition on grain surfaces, we also performed similar observation, using different samples. Figure. 4.7 shows examples of such similar observations under much-higher water vapor pressure. Points 7A and 7B in Fig. 4.5 indicate the conditions in Fig. 7A and 7B, respectively. We raised temperature from −1.2 to −0.9 °C (P_e= 568 Pa) under water vapor pressures 624 Pa (Fig. 4.7A) and 646 Pa (Fig. 4.7B). Irrespective of water vapor pressure, we could confirm the appearance and subsequent disappearance of droplet-type QLLs in a similar way, although the temperature was slightly different to Fig. 4.6.

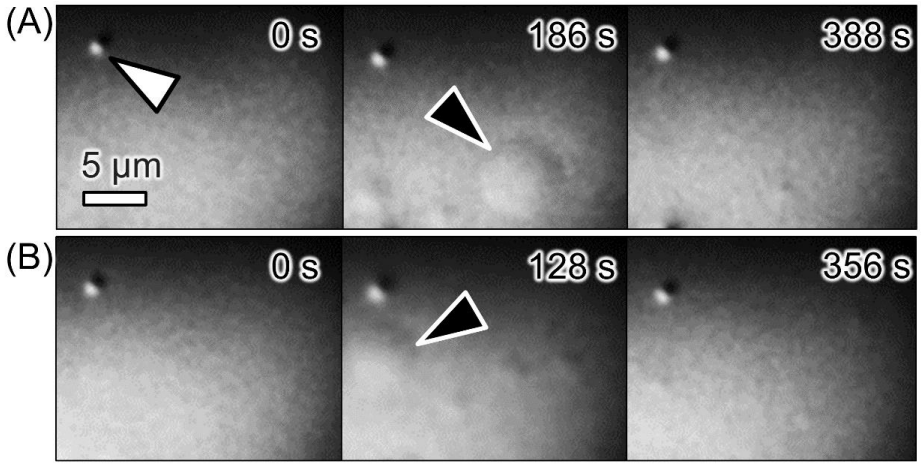

Fig. 4.7. The emergence and subsequent disappearance of droplet-type QLLs on surfaces of ice grains, at −0.9 °C (P_e= 568 Pa). The sample shown un this figure was different from that shown in Fig. 4.6. Panels A and B present time course of LCM-DIM images of the grain surfaces at (A) P= 624 Pa and (B) P= 646 Pa, respectively. These P-T conditions correspond to the points 7A and 7B in Fig. 4.5. After temperature was raised from −1.2 °C to −0.9 °C, the droplet-type QLLs (marked by black arrowheads) appeared on the grain surface within a couple of minutes, however subsequently disappeared gradually from the grain surface as further time elapsed. The temperature increase from −0.9 to −0.6 °C occurred within 1 min. In images A and B, the time 0 s corresponds to the moment at which temperature was started to increase. A polystyrene particle located on the grain surface is indicated by a white arrowhead.

4-2-2 Thin-layer-type QLLs

On the surfaces of ice single crystals, thin-layer-type QLLs of 9 nm in thickness appear in addition to the droplet-type QLLs [42, 43]. However, on the grain surfaces of the polycrystalline ice thin films, it was very difficult to find the emergence of thin-layer-type QLLs. Among all observations, we succeeded in observing thin-layer-type QLLs just three times for limited duration times. This was mainly due to the fact that the grain surfaces of the polycrystalline ice thin films were significantly rougher than basal and prism faces of ice single crystals.

Figure. 4.8 shows only one observation that allowed us to prepare relatively clear still images of thin-layer-type QLLs on the grain surfaces. In Fig. 4.8A1, a thin-layer-type QLL (red arrowhead) appeared on a grain surface, and moved in a direction marked by a red arrow. As time elapsed, the thin-layer-type QLL shown in Fig. 4.8A1 moved to the right side of the field of view, and two thin-layer-type QLLs newly appeared in the left side (Fig. 4.8A2). A half-black/white arrowhead shows a hole formed just above a polystyrene particle buried inside the grain surface during the growth: this can be a reference point. As shown in Fig. 4.8B, we could also observe the coalescence of adjacent thin-layer-type QLLs at the point marked by the black arrow. In the three-time observations, the appearance temperatures of the thin-layer-type QLLs were −0.9, −0.9 and −0.3 °C (−0.7±0.3 °C). Because of the experimental difficulty in visualizing the thin-layer-type QLLs on the grain surfaces, at this moment we have no experimental datum concerning the disappearance and water-vapor-pressure dependence of the thin-layer type QLLs.

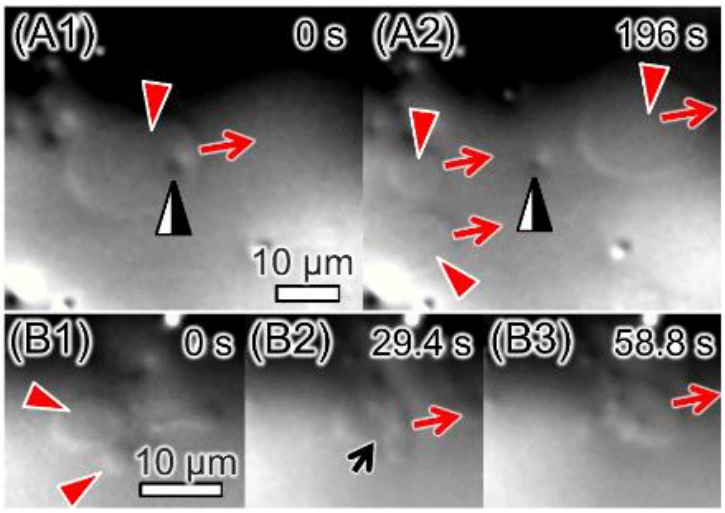

Fig. 4.8. The emergence of thin-layer-type QLLs on grain surfaces at T= −0.9 °C (P_e=568 Pa) and P=593 Pa. (A) A thin-layer-type QLL (red arrowhead) appeared on a grain surface (image A1) and moved in the red-arrow direction. In the image A2, the thin-layer-type QLL shown in the image A1 moved to the right side of the field of view, and two thin-layer-type QLLs newly appeared in the left side. A half-black/white arrowhead represents a whole formed just above a polystyrene particle buried inside the grain surface during the growth. (B) Two adjacent thin-layer-type QLLs (read arrowheads) coalesced with each other at the point marked by the black arrow. In these images, the time of 0 s only shows the moments at which images A1 and B1 were taken, and hence does not correspond to the duration time after the temperature change. Since all panels show magnified images, no grain boundary is shown in the images.

4-3. Discussion

4-3-1. A variation of critical temperatures above which QLLs could appear

We summarized the critical temperatures above which QLLs could appear in grooves of grain boundaries and on grain surfaces in Fig. 4.9A and 4.9B, respectively. Since the number of successful visualization of thin-layer-type QLLs is very limited (only three times), we do not show the data of thin-layer-type QLLs in Fig. 4.9.

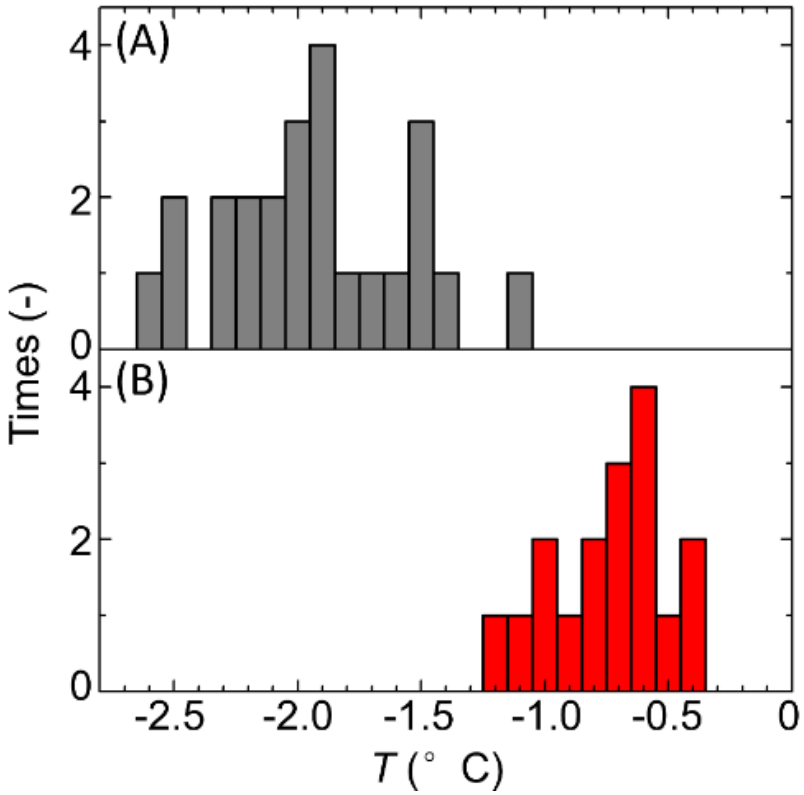

Fig. 4.9. Two temperature ranges at which specific events occurred in grain boundaries (A: −1.9±0.4 °C) and on grain surfaces (B: −0.7±0.2 °C), respectively. (A) The variation of the temperature above which QLLs whose volume was sufficient to move the particles appeared in grooves of grain boundaries. (B) The variation of the temperature above which droplet-type QLLs appeared on grain surfaces but soon disappeared.

Figure 4.9A shows the summary of 22 runs: the variation in the particle-moving temperature probably corresponds to the variation in the characters of grain boundaries. This issue is an important subject in future studies. Note that all polystyrene particles, which we observed in the grooves of the grain boundaries, showed the movement in the grooves with increasing temperature. This result demonstrates that all particles were located not inside the grain boundaries but on the surfaces of the grooves: the particles were rejected by the growing ice-water interfaces [73] and then segregated on the groove surfaces during the sample preparation. Hence, we could observe the particles located on the groove surfaces, although the focus depth of the LCM-DIM (7.5 μm) [57] was not sufficient to distinguish whether the particles were on the surface or inside. However, we cannot exclude the possibility in which the particles were "partly trapped" on the groove surfaces, which could also cause the significant variation shown in Fig. 4.9A.

Figure 4.9B shows a summary of 17 runs: the variation of the temperature (−0.7±0.2 °C), above which droplet-type QLLs appeared on grain surfaces but soon disappeared. This variation in the temperature is probably due to the variation in face indices of grain surfaces. Grain boundaries induced the formation of QLLs at a lower temperature than grain surfaces.

4-3-2. QLLs in grooves of grain boundaries

In the section 4-1-2, we concluded that QLLs in grooves of grain boundaries were mainly supplied by grain boundaries. In this section, we explain the formation mechanisms of QLLs in grooves. Figure. 4.10 shows the relation between the free energies of an ice crystal (Ice), a grain boundary (G.B.), a grain surface (G.S.), QLLs in the grain boundary, and QLLs in the groove of the grain boundary (G.G.). On basal faces of ice single crystals, we previously reported that droplet-type and thin-layer-type QLLs exist kinetically as metastable phases in the blue and red *P-T* ranges in Fig. 4.5 [46, 47]. In this study, we apply the same concept. Therefore, the QLLs on the grain

surface (QLLs on G.S.) are thermodynamically more unstable (stable) than the ice crystal in supersaturated (undersaturated) conditions.

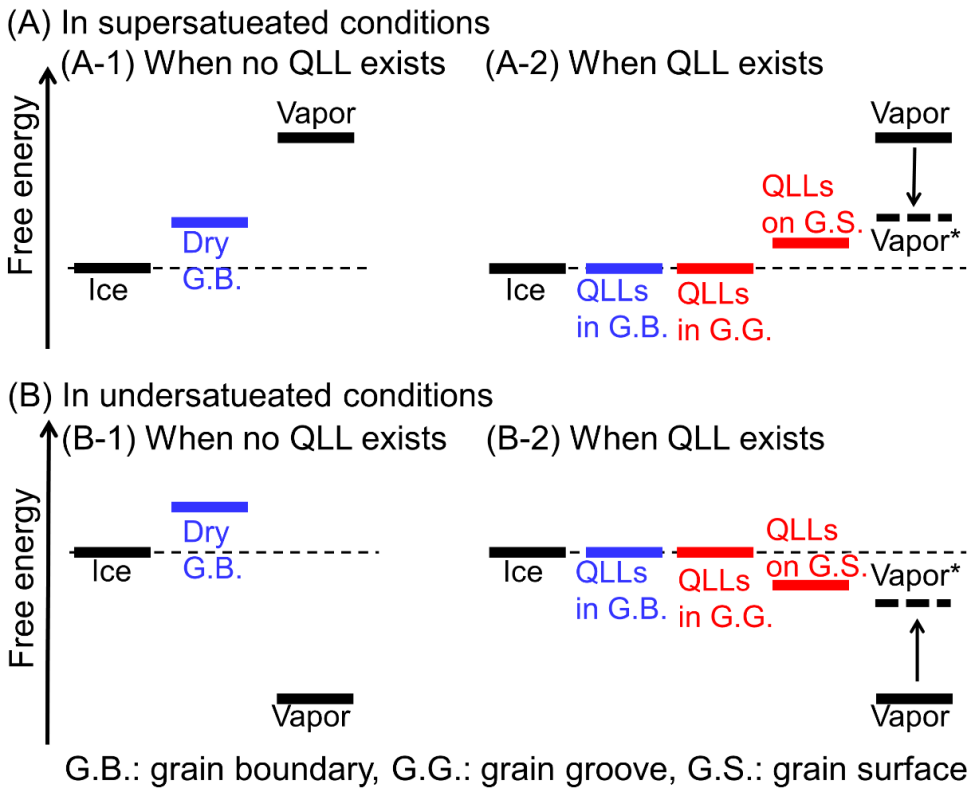

Fig. 4.10. Free-energy diagrams for individual phases in (A) supersaturated and (B) undersaturated conditions, when QLLs (1) do not exist and (2) exist. The abbreviations G.B., G.G., and G.S. denote a grain boundary, a groove of a grain boundary, and a grain surface, respectively. (A-1 and B-1) Because a grain boundary (a two-dimensional object) is not a phase, a dry grain boundary (Dry G.B.) here indicates a grain boundary and adjacent ice thin layers (slabs) in which the strain energy of the grain boundary is distributed. (A-2 and B-2) With increasing temperature, the dry grain boundary is melted and QLLs are formed in the grain boundary. QLLs in G.B. show QLLs formed by the melting of the ice thin layers adjacent to the dry grain boundary. QLLs in G.G. present QLLs that appeared in a groove of a grain boundary. QLLs on G.S. indicate QLLs formed on a grain surface. The free energy level named Vapor* shows a water vapor pressure depleted (or enriched) by QLLs in a groove of a grain boundary.

In general, grain boundaries are significantly more unstable than a crystal, because lattice mismatches, which are caused by the contacts of adjacent ice grains with different crystallographic orientations [61-63], form strain energy. In Fig. 4.10, because a grain boundary (a two-dimensional object) is not a phase, here a dry grain boundary (Dry G.B. in Figs. 4.10A-1 and 4.10B-1) indicates a grain boundary and adjacent ice thin layers (slabs) in which the strain energy of the grain boundary is distributed. After a dry grain boundary is melted with increasing temperature, QLLs thus formed in the grain boundary (QLLs in G.B. in Figs. 4.10A-2 and 4.10B-2) significantly relax the lattice mismatches. Hence, the QLLs in the grain boundary are as stable as the ice crystal. In such case, it is reasonable to assume that the QLLs formed in the groove of the grain boundary (QLLs in G.G.) are also as stable as the QLLs in the grain boundary, because the QLLs in the grain boundary and the QLLs in the groove are formed even in the equilibrium condition. Hence, after the dry grain boundary is melted, the QLLs in the grain boundary and the QLLs in the groove become thermodynamically stable. Although the QLLs in the grain boundary supply the QLLs in the groove, we distinguished these QLLs, because in the QLLs two phases (the QLLs and the ice crystal) coexist in the grain boundary, whereas three phases (the QLLs, the ice crystal and the water vapor) coexist in the QLLs in the groove.

We speculated that such grain boundary melting occurred continuously with increasing temperature: i.e. if we use polystyrene particles with a smaller diameter, we should detect the movement of the particles at temperature lower than −2.3 °C, although at present we have no experimental evidence. In this study, the amount of the QLLs in the grooves of the grain boundaries was not sufficient to determine the water level of the QLLs in the grooves using the LCM-DIM and the Linnik interferometer: the spillover of the QLLs from the grooves of the grain boundaries did not occur.

So far, two experimental studies were reported on the behavior of QLLs in grain boundaries of polycrystalline ice. Lu et al. concluded that grain boundary width was on the order of a few nanometers at −2 °C, and that premelting of grain boundary was implausible at this temperature [52]. In addition, Thomson et al. also reported that the thickness of grain boundaries was in the range of 1-10 nm at undercooling of ~1.5 K

[68]. However, Fig. 4.2 indicates that to observe the movements of the particle in the groove of the grain boundary, openings wider than the diameter of the particles (653 nm) needed to be filled with the QLLs. Hence, there existed the possibility that the thickness of the grain boundaries was much wider than those reported by Lu et al. [52] and Thomson et al [68]. Our optical microscope system used in this study was a reflection type. Hence, we could not obtain any information from inside of the grain boundaries. To further study the inside of the grain boundaries, now we are planning to develop a transmission-type optical system combined with the present setup.

4-3-3. QLLs on grain surfaces

In this section, we also explain the appearance and disappearance of droplet-type QLLs on grain surfaces. In the pressure range marked by the double-headed green arrow in Fig. 4.5, the disappearance of the droplet-type QLLs on the grain surfaces does not conflict with the results obtained on basal faces of ice single crystals. Because the droplet-type QLLs (a metastable phase) are more unstable than the ice crystal (the most stable phase), the ice grains grew consuming the QLLs on the grain surfaces. However, we could also observe the disappearance of QLLs on grain surfaces even in the blue and red *P*-*T* regions in Figs. 4.1 and 4.5. At present, the reason for this discrepancy is unclear, however we propose the following two possible causes.

One possible cause is grain surfaces whose crystallographic orientations were random. Because such grain surfaces have a significantly-higher kink density than basal faces of ice single crystals, the grain surfaces should grow via the adhesive-growth mechanism, which is usually significantly faster than the layer-by-layer growth [74]. Hence, the grain surfaces in contact with the droplet-type QLLs probably showed melt growth with significantly faster speed than basal faces, resulting in the disappearance of the droplet-type QLLs on the grain surfaces. In other words, the supersaturation and undersaturation of water vapor probably needed to be much higher to keep the droplet-type QLLs on the grain surfaces kinetically. To prove this scenario, we tried to further

increased water vapor pressure to perform similar observations. However, because of much higher driving force determined by $kT \cdot \ln(P/P_e)$ for both QLLs and polycrystalline ice thin films, with further increasing supersaturation, the number and size of the droplet-type QLLs on the grain surfaces increased and decreased significantly. In addition, grain surfaces also became significantly rough. Resultantly we could not distinguish any events on the grain surfaces because of the limited spatial and temporal resolutions of our optical microscopy system.

The other possible cause is the appearance of the QLLs at $T_{sample} \geq -1.9 \pm 0.4$ °C in the grooves of the grain boundaries (Fig. 4.2). Hence, at $T_{sample} = -0.6$ °C, the droplet-type QLLs formed on the grain surfaces coexisted with the QLLs located in the grooves of the grain boundaries. As shown in the free energy diagram (Figs. 10A-2 and 10B-2), in a supersaturated (undersaturated) condition, the free energy of the QLLs on the grain surface (QLLs on G.S.) is higher (lower) than that of the ice crystal, because the QLLs on the grain surface are a metastable phase [46, 47]. If the amount of QLLs in the grooves is much larger than the amount of the droplet-type QLLs on the grain surfaces, the QLLs in the grooves can dominate P distribution on the polycrystalline ice surfaces. Under a supersaturated (undersaturated) condition, the growth (evaporation) of the QLLs in the grooves can deplete (enrich) P in the vicinities of the grooves, and can eventually decrease (increase) P on the grain surfaces: see the free energy levels Vapor* (thick dotted lines) in Fig. 4.10, resulting in the decrease in the driving force for the growth of the droplet-type QLLs on the grain surfaces. To probe this scenario, we need to further study the P distribution on the polycrystalline ice surfaces experimentally.

In addition to the disappearance of the QLLs on the grain surfaces, we also need to explain their appearance: i.e. nucleation. As shown in Fig. 4.6, we could observe the appearance of the droplet-type QLLs even in the vicinity of the vapor-ice equilibrium curve. This result implies that on the grain surfaces the nucleation of the QLLs was enhanced compared to that on basal faces. As already explained, the grain surfaces have a much higher kink density than basal faces. Hence, it is reasonable to assume that such high-kink-density surfaces are more liquid like than basal faces and then have a smaller

solid-liquid interfacial free energy. To probe this scenario, we need to perform precise nucleation experiments in the future.

4-4. Summary

In this chapter, we observed polycrystalline ice thin films using the LCM-DIM. On the basis of the observed macroscopic fluidity, we determined the presence of QLLs. Our key results are summarized as follows.

(1) With increasing temperature, the QLLs, which had sufficient volume to move the polystyrene particles, preferentially appeared in the grooves of grain boundaries at −1.9 ± 0.4 °C. The appearance of such QLLs was observed irrespective of the water vapor pressure (even at the vapor−ice equilibrium condition), indicating that these QLLs were formed by melting of the grain boundaries to eliminate the lattice mismatch between grains. After the QLLs appeared in the grooves, the QLLs continued to exist.

(2) With increasing temperature, the droplet-type QLLs appeared kinetically on the grain surfaces at −0.7 ± 0.2 °C. However, they could not continuously exist on the grain surfaces and disappeared within 5 ± 3 min even though the temperature and water vapor pressure were kept constant. Hence, after the disappearance of the droplet-type QLLs, the grain surfaces were dry. These results suggest that the droplet-type QLLs on the grain surfaces were a metastable phase, like those on ice single-crystal surfaces.

(3) With increasing temperature, thin-layer-type QLLs also appeared on the grain surfaces at temperatures higher than −0.7 ± 0.3 °C. However, because of the difficulty in visualizing these QLLs on rough grain surfaces, we have no data concerning their disappearance or water-vapor-pressure dependence.

5. Surface melting just below the melting point

In this chapter we show phenomena observed in a temperature range higher than that in the chapter 4. First, we show the emergence of a large amount of QLL from grain boundaries in the section 5-1. Then we explain the difference between surface melting of polycrystalline ice thin films and that of ice single crystals just below the melting point in the section 5-2. Next, we discuss a temperature distribution in a polycrystalline ice thin films and an origin of QLLs in the section 5-3. Finally, we summarize the results in the section 5-4.

5-1. Emergence of a large amount of QLLs from grain boundaries

To investigate the behavior of QLL at a temperature close to the melting point (0 °C), we further increased the temperature of polycrystalline ice thin films (T_{sample}). Then we investigated, using LCM-DIM, whether there exists any difference in the appearances of QLLs on polycrystalline ice thin films and on ice single crystals. Figure. 5.1A shows a typical LCM-DIM image of a polycrystalline ice thin film at T= −0.5 °C (P_{e}= 587 Pa) and P= 646 Pa. On grain surfaces there was no QLL that exhibited macroscopic fluidity, as we explained in the chapter 4. However, after we raised T to −0.2 °C from −0.3 °C (Fig. 5.1B) under the constant P, surprisingly a large amount of QLLs quickly emerged from grain boundaries (Figs. 5.1B-D), and finally fully covered the surface of the polycrystalline ice thin film within 70 s.

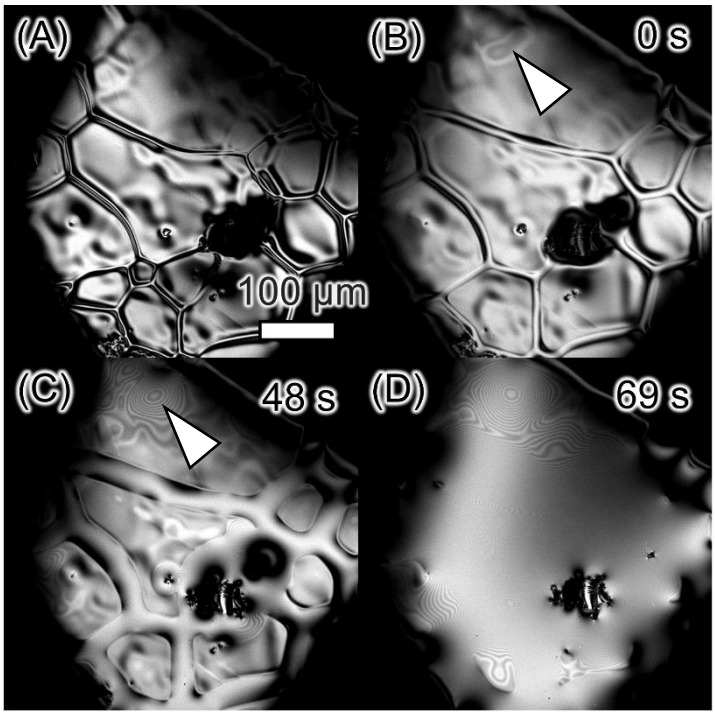

Fig. 5.1. Surface melting of a polycrystalline ice thin film just below the melting point (0 °C). (A) An LCM-DIM image of dry grain surfaces at T= −0.5 °C (P_e= 587 Pa) and P = 646 Pa. QLLs existed only in grooves of grain boundaries, as explained in the chapter 4. (B-D) LCM-DIM images when T was raised from −0.3 °C (P_e= 596 Pa) to −0.2 °C (P_e= 601 Pa) under the constant P (= 646 Pa). A large amount of QLLs emerged from the grain boundaries. Then the QLLs fully covered the polycrystalline ice thin film within 70 s. (B and C) Counter lines marked by white arrowheads indicate that a QLL already existed on the grain surfaces at T= −0.3 °C. In images B-D, a time of 0 s corresponds to the moment at which the temperature was started to increase.

In Fig. 5.1D, the fucus position was set at the air-QLL interface, as schematically shown in Fig. 5.2A. Then, to check whether the polycrystalline thin film was entirely melted, we moved the focus position toward the inside of the QLL. Then we found that the ice grains and grain boundaries that were observed in Fig. 5.1A still remained beneath the QLL newly appeared, as shown in Fig. 5.2B. In Fig. 5.2B, the focus position was set at the inside of the ice grains, as schematically shown in Fig. 5.2A. Note that T_{sample} was still below the melting point.

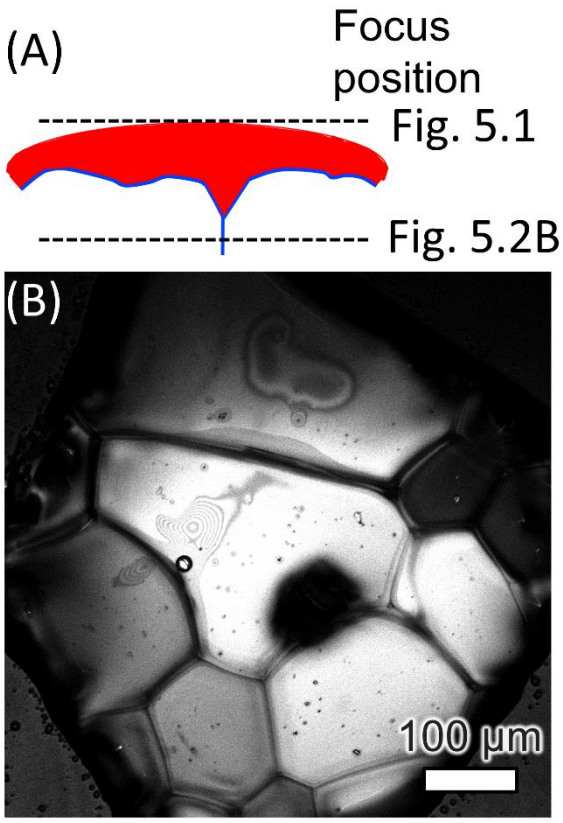

Fig. 5.2. A polycrystalline thin film after its surface was fully covered with QLL at −0.2 °C (P_e= 601 Pa) and P = 646 Pa. (A) A schematic of focus positions. The upper dashed line shows a focus position in Fig. 5.1: at the interface of the QLL and vapor. The lower dashed line presents a focus position of the image B. (B) When the focus position of the LCM-DIM was set at the inside of the QLL, the ice grains and grain boundaries observed in Figs. 5.1A-C still remained beneath the QLL shown in Fig. 5.1D.

In order to clarify whether the phenomena found in Figs. 5.1 and 5.2 were bulk melting, we further raised T_{sample} gradually. Figure 5.3 shows a time course of LCM-DIM images of a polycrystalline ice thin film. In these images, the focus was set at the inside of the polycrystalline thin film. As shown in Fig. 5.3, the ice grains shrank quickly, and disappeared within 6 min at T_{sample} = 0 °C. Therefore, we concluded that the melting of the polycrystalline ice thin film shown in Fig. 5.3 corresponds to the bulk melting occurred at 0 °C. Note that the emergence of the large amount of the QLLs

from the grain boundaries (Fig. 5.1) is fully different from the bulk melting of the polycrystalline ice thin film (Fig. 5.3).

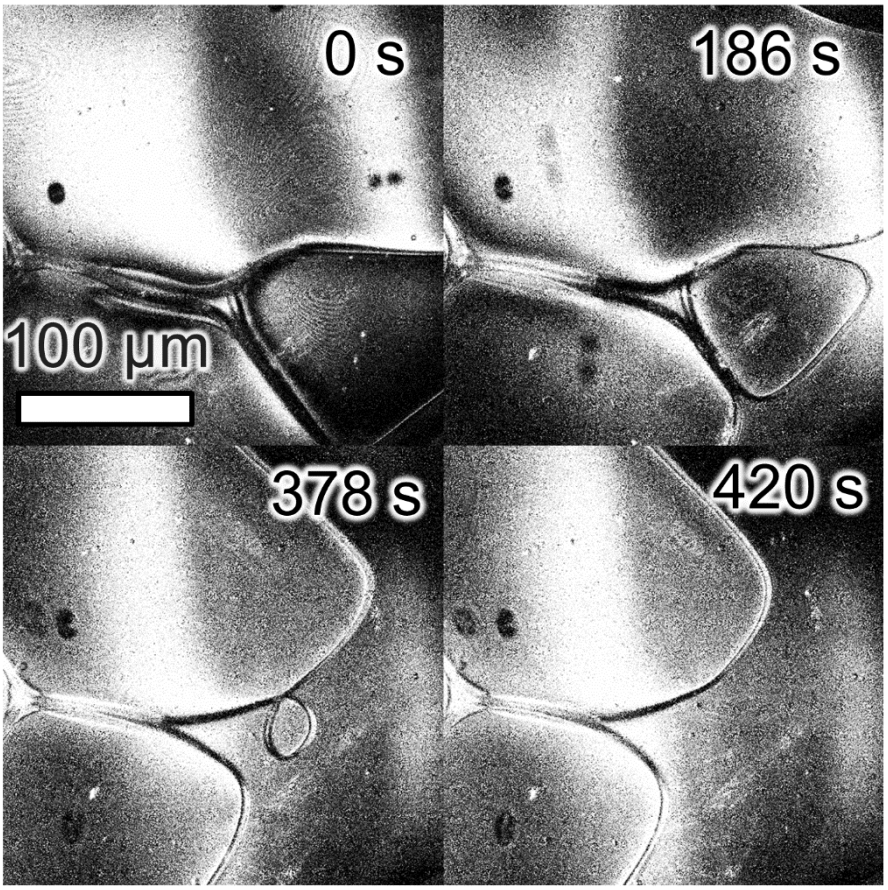

Fig. 5.3. Bulk melting of a polycrystalline ice thin film. A focus position of LCM-DIM was set at the inside of the polycrystalline ice thin film. When T_{sample} was increased to the melting point (0 °C), ice grains shrank quickly and one of the ice grains disappeared within 6 min. A time of 0 s corresponds to the moment at which the temperature became constant at 0 °C.

5-2. Difference in surface melting of polycrystalline ice thin films and ice single crystals

For comparison, we also observed the behaviors of QLLs on surfaces of ice single crystals at a temperature very close to melting point. Figure 5.4 shows a typical LCM-DIM image of a basal face of an ice single crystal at $T_{sample} = -0.2$ °C ($P_e = 601$ Pa) and

P= 646 Pa. Although a large area of the basal face was covered with droplet-type QLLs, a solid-vapor interface that was still not covered with the droplet-type QLLs remained. Notice that T_{sample} and P in Fig. 5.4 were completely the same as those in Fig. 5.1D (for the polycrystalline ice thin film). In contrast, as shown in Fig. 5.1, the surface of the polycrystalline ice thin film was fully covered with the QLLs emerged from the grain boundaries within 70 s. In other words, the speed of the coverage of the polycrystalline ice thin film with the QLL was significantly faster than that of the basal face.

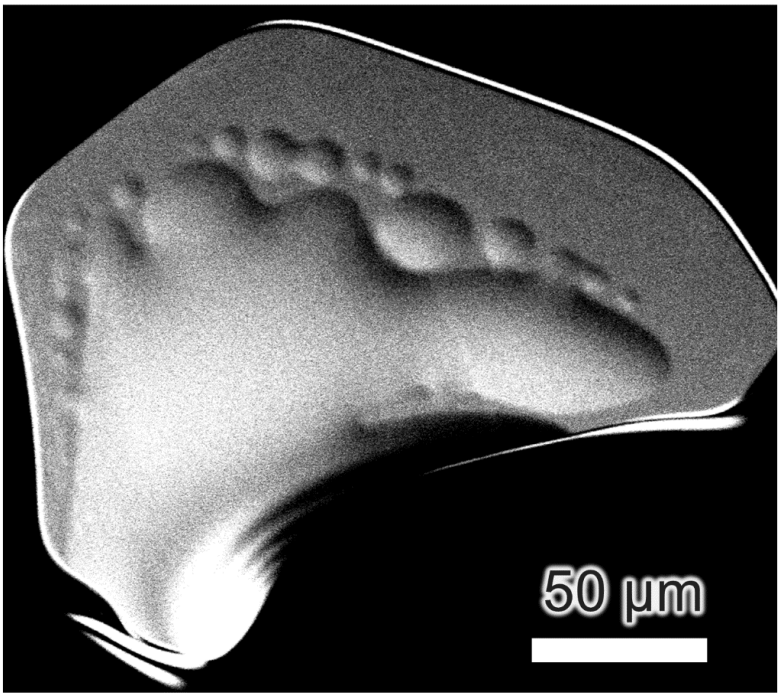

Fig. 5.4. Surface melting of a basal face of an ice single crystal at T= −0.2 °C (P_e= 601 Pa) and P= 646 Pa. A typical LCM-DIM image shows that a large volume of droplet-type QLLs existed on the basal face, but the basal face that was not covered with the droplet-type QLLs still stably remained. The values of T_{sample} and P were completely the same as those in Fig. 5.1D (for the polycrystalline ice thin film).

In addition, in Fig. 5.1C, interference fringes (marked by a white arrowhead) spontaneously appeared on the grain surface. This result shows that QLLs were formed also on the grain surface: the interference fringes were formed by the interference of a light beam reflected from an air-QLL interface and that reflected from a QLL-ice interface. Hence, the interference fringes correspond to contour lines of the QLL

appeared on the grain surface. As time elapsed, the contour lines developed relatively homogeneously on the grain surface (Figs. 5.1C-D). In addition, we could not observe any droplet-type QLL on the grain surface. Therefore, from the results shown in Figs. 5.1 and 5.4, we concluded that the free energy of the interface between the QLLs and the polycrystalline ice grain was significantly smaller than that between the QLLs and the basal face. This strongly supports the discussion about a solid-liquid interfacial free energy in the section 4-3-3.

5-3. Discussion

5-3-1. Distribution of temperature

To prove whether the emergence of the large amount of QLL from the grain boundary (Fig. 5.1) was not due to the bulk melting but was due to the surface melting, we need to confirm that the temperature of the surface of the polycrystalline ice thin film was certainly below the melting point (0 °C). If there exist a temperature distribution in the vertical direction (normal to the thin film), and then if the temperature of a sample surface is higher than 0 °C, such sample surface is melted by the bulk melting and then the melting is stopped when the position of the polycrystalline ice thin film reaches 0 °C, as schematically shown in Fig. 5.5.

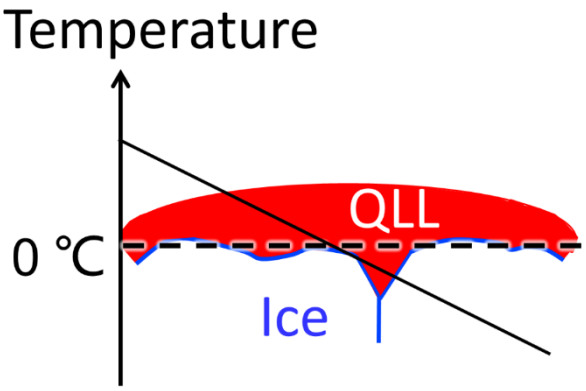

Fig. 5.5. A schematic of a temperature distribution in the vertical direction (normal to the polycrystalline thin film). If a temperature distribution exists in the vertical direction, and also if the temperature of the sample surface is higher than 0 °C, the surface of the polycrystalline thin film is melted by the bulk melting.

To deny such possibility, we need to directly measure the temperature of a sample surface. However, it was experimentally difficult. Hence, we calculated a vertical temperature distribution in a sample ice, assuming the conduction of heat in one dimension. For details of the calculation, see Appendix C. As a result of the calculation, we found that even when the temperatures of the upper and lower Cu plates (T_{top} and T_{bottom}) are −0.5 and +100 °C, respectively, the temperature difference between the surface and bottom of a sample ice thin film of 70 μm in thickness is less than 0.03 °C. In addition, under a realistic condition (T_{top} = −0.5 and T_{bottom} = +1.0 °C), the temperature difference is less than 0.0001 °C. These calculations strongly suggest that the temperature difference between the surface and bottom of the sample ice thin film was negligibly small, and that the phenomena observed in Fig. 5.1 was due to the surface melting of the polycrystalline ice thin film.

5-3-3. Origin of QLLs on polycrystalline ice thin films

The surface melting of the polycrystalline ice thin films shows significant

differences to that of ice single crystals just below the melting point. To clarify what was the origin of the large amount of QLLs appeared on the polycrystalline ice thin film, next we observed the emergence of QLLs at a temperature close to the melting point, using the Linnik interferometer.

Figures 5.6A(1) and B(1) respectively show an LCM-DIM image and an interferometry image of a polycrystalline ice thin film at T_{sample} = −0.4 °C (P_e= 591 Pa) and P = 556 Pa (undersaturation, σ= 0.93). When we raised T_{sample} to −0.2 °C at the constant P (σ = 0.92), a shape of interference fringes was significantly changed, as shown in Fig. 5.6B(2-4). Figure 5.6B(4) was taken after the polycrystalline ice thin film was fully covered with QLLs at −0.2 °C, as shown in an LCM-DIM image (Fig. 5.6A(2)).

In order to compare the changes in the shapes of the interference fringes on a groove of a grain boundary and those on a grain surface, we prepared time-space plots. Figures. 5.6C and D show the movements of the fringes in a grain boundary and on a grain surface, respectively. During the increase in T_{sample}, the height (water level) of the QLL in the grain boundary increased significantly (Fig. 5.6C). In contrast, the height of the grain surface remained almost constant or decreased slightly by sublimation (Fig. 5.6D). These results clearly show that the large amount of QLLs was formed mainly by the melting of the grain boundary and then finally covered the surface of the polycrystalline ice thin film. To prove this scenario quantitatively, we need to further perform similar observations under various P in the future. However, Fig. 5.6 clearly demonstrates that grain boundaries dominate surface melting of ice, in particular at a temperature close to the melting point.

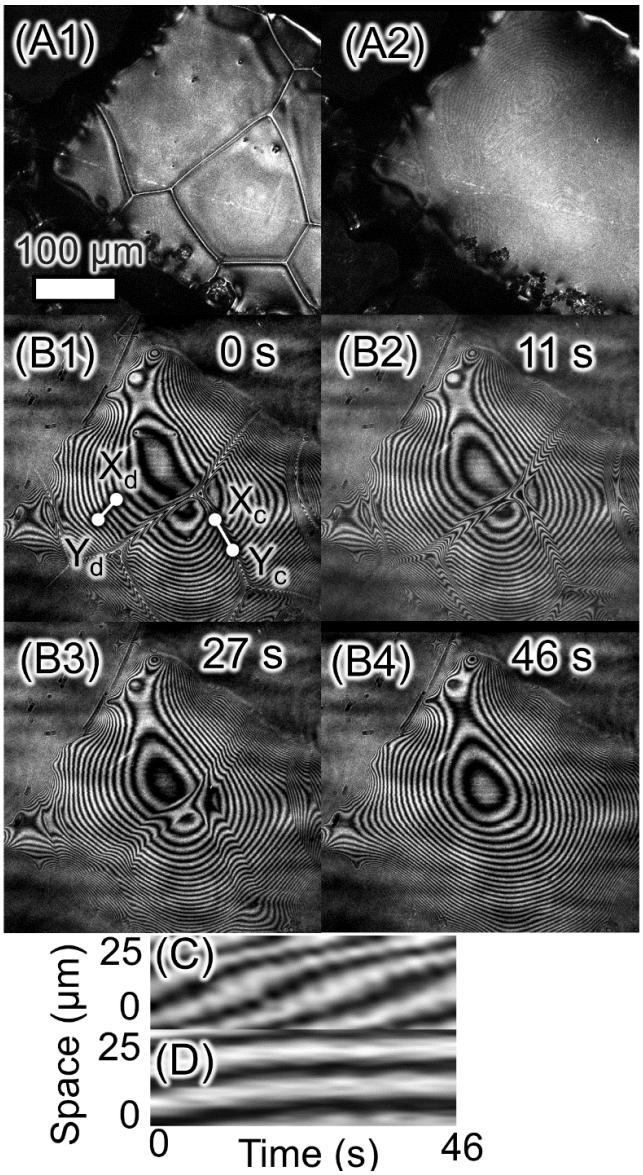

Fig. 5.6. Interferometric observation of a polycrystalline thin film just below the melting point (0 °C), using a Linnic interferometer. (A1) and (A2) LCM-DIM images that were taken before and after the temperature change from −0.4 °C (P_e= 591 Pa) to −0.2 °C (P_e= 601 Pa) under a constant P= 556 Pa, respectively. Grain surfaces shown in (A1) were still dry, but those in (A2) were fully covered with a QLL emerged newly. (B1-B4) Interferometric images during the increase in T from −0.4 to −0.2 °C under the constant P. A time of 0 s corresponds to the moment at which the temperature was started to increase. (C) and (D) Time-space plots taken along the lines X_c-Y_c and X_d-Y_d in (B1), respectively showing the movements of the interference fringes in a grain boundary and on a grain surface during the temperature change shown in (B1)-(B4).

5-4. Summary

In this chapter, we observed the polycrystalline ice thin films, using LCM-DIM, under a temperature just below the melting point (0°C). Our key results are summarized as follows.

(1) When we increased the temperature of the polycrystalline ice thin film to −0.2 °C, the large amount of QLL was emerged from the grain boundaries and then fully covered the surface of the thin film within 70 s. However, the ice grains and grain boundaries still remained beneath the QLL. In contrast, when we further increased the temperature to 0 °C, the polycrystalline ice thin film fully disappeared within 6 min. These results indicate that the emergence of the large amount of QLL at −0.2 °C was not due to the bulk melting but due to the surface melting of the polycrystalline ice thin film.

(2) In addition to the emergence of the large amount of the QLL from the grain boundaries at −0.2 °C, QLLs were also spontaneously formed on the grain surfaces immediately after the temperature increase. In contrast, on the basal face of the ice single crystal, the solid-vapor interfaces that was still not covered with the droplet-type QLLs remained at least within 80 s. These results strongly suggest that the free energy of the interface between the QLLs and the polycrystalline ice grain was smaller than that between the QLLs and the basal face.

6. Conclusions

In this study, surface melting of polycrystalline ice below the melting point (0 °C) of ice was investigated. Surfaces of polycrystalline ice thin films were observed, using a laser confocal microscope combined with a differential interference contrast microscope (LCM-DIM), a Linnik interferometer and a Michelson interferometer, under various temperatures and water vapor pressures.

In Chapter 3, behavior of grains in polycrystalline ice thin films was investigated. Observation using a polarized light microscope with an objective of a thick focal depth (170 μm) revealed that the grains were randomly oriented in the polycrystalline ice thin film. LCM-DIM observation of the polycrystalline ice thin film demonstrated that some grains exhibited relatively fast grain growth on a time scale of approximately 30 min. To eliminate the effects of the grain growth, the grains that exhibited the relatively fast grain growth were excluded from further investigations of the surface melting of the polycrystalline ice thin films.

In Chapter 4, the formation of quasi-liquid layers (QLLs) in grooves of grain boundaries and on grain surfaces was investigated. LCM-DIM observation indicated that with increasing temperature, QLLs, which had sufficient volume to move polystyrene particles, preferentially appeared in grooves of grain boundaries at −1.9 ± 0.4 °C. After the QLLs appeared in the grooves, the QLLs continued to exist. The appearance of such QLLs was observed irrespective of the water vapor pressure (even at the vapor−ice equilibrium condition). These results demonstrate that QLLs in grooves are formed by melting of grain boundaries to eliminate lattice mismatches between adjacent grains. In addition, with further increasing temperature, the droplet-type QLLs appeared on the grain surfaces at −0.7 ± 0.2 °C. However, they could not continuously exist on the grain surfaces and disappeared within 5 ± 3 min even though the temperature and water vapor pressure were kept constant. These results strongly suggest that droplet-type QLLs on grain surfaces are a metastable phase, like those on ice single crystal surfaces, and that they are formed kinetically. Although the reason for the disappearance of the QLLs on the gran surfaces is still unclear, two possible causes,

based on faster growth of grain surfaces and changes in distribution of water vapor pressure in the vicinity of the grain surfaces, were proposed. Moreover, thin-layer-type QLLs also appeared on the grain surfaces at temperatures higher than −0.7 ± 0.3 °C. However, because of the difficulty in visualizing these QLLs on rough grain surfaces, there is no datum concerning their disappearance and water-vapor-pressure dependence.

In Chapter 5, the behavior of QLLs at temperatures very close to the melting point was investigated on polycrystalline ice thin films. LCM-DIM observation revealed that with increasing temperature to −0.3 ± 0.1 °C, a large amount of QLLs spontaneously emerged preferentially from grooves of grain boundaries, and then fully covered the surfaces of the polycrystalline ice thin films within 70 s. Because all ice grains still remained solid (unmelted) beneath the QLLs, it was not bulk melting. In contrast, on basal faces of ice single crystals, with increasing temperature to the same −0.3 ± 0.1 °C, droplet-type QLLs appeared, but the basal faces were not fully covered with the QLLs within 80 s. The difference between the appearances of QLLs on the polycrystalline ice thin films and the basal faces suggests that wettability of surfaces of the polycrystalline ice thin films is significantly higher than that of basal faces. Interferometry observations strongly suggests that at temperatures just below the melting point, QLLs on polycrystalline ice thin films are formed mainly by the melting of grain boundaries.

There still exist several works that should be performed in the future to further clarify the surface melting of polycrystalline ice thin films. (1) The relation between characters of grain boundaries and onset temperature of the formation of QLLs in grooves of the grain boundaries needs to be investigated experimentally. A polarized light optical microscopy system, which can determine the orientations of crystallographic *c*-axes of individual grains, is now under development. (2) In addition, the reason for the disappearance of droplet-type QLLs on grain surfaces at −0.7 ± 0.2 °C also needs to be investigated in detail. To perform such study, the growth of grain surfaces beneath QLLs and distribution of water vapor in the vicinity of the polycrystalline ice thin film have to be measured experimentally. (3) Furthermore, to investigate whether the QLLs that fully covered the surfaces of the polycrystalline ice thin films at −0.3 ± 0.1 °C were formed by the melting of the grain boundaries,

interferometry observation needs to be performed under a wide range of supersaturation/undersaturation.

At present, surface melting of polycrystalline ice still has many open questions. However, to my knowledge, this is the first study that directly revealed the formation of macroscopically fluidic QLLs on polycrystalline ice. This study clearly demonstrates that the behavior of QLLs on polycrystalline ice is significantly different from that on an ice single crystal. In particular, it was found that grain boundaries play a more important role in the surface melting of polycrystalline ice than grain surfaces. The results obtained in this study are expected to contribute significantly to future studies on surface melting of polycrystalline ice.

Appendix

A. The conventional picture of surface melting

Lacmann and Stranski first gave a thermodynamic explanation for the wetting of ice crystal surfaces with QLLs [29]. Then Kuroda and Lacmann developed this idea into an explanation of the morphologies of snowflakes [30, 31]. Kuroda and Lacmann assumed that one QLL phase fully covers an ice surface at the solid−vapor equilibrium water vapor pressure. The thickness of QLLs is, at most, on the order of several tens of nanometers [11]. Hence, free energies of interfaces play a crucial role, in addition to those of bulk phases. As a rough approximation, Kuroda and Lacmann presumed bulk free energy of QLLs to be that of liquid water. It is still unclear whether their approximation is appropriate. However, it seems reasonable to assume that the bulk free energy of QLLs is higher (less stable) than that of ice crystals. When there is no QLL (Fig. 1.2A), there exists one interface between ice and vapor. In contrast, when an ice surface is covered with a QLL (Fig. 1.2B), there exist two interfaces: a QLL−ice interface and a QLL−vapor interface. The free energy of a QLL−ice interface is smaller (more stable) than that of an ice−vapor interface, because the structures of a QLL and an ice are more similar than those of an ice and vapor. In addition, the free energy of a QLL−vapor interface is also smaller (more stable) than that of an ice−vapor interface, for the same reason. Therefore, Kuroda and Lacmann assumed that there should exist a case in which the sum of the free energies of QLL−ice and QLL−vapor interfaces is smaller (more stable) than the free energy of an ice−vapor interface: an ice crystal surface is fully wetted with a QLL (complete wetting). Kuroda and Lacmann evaluated the wettability of a QLL on ice crystal surfaces using values of interfacial free energies determined previously [31], which lead to the expectation that the assumption of complete wetting was valid. Taking into account the contributions of both a bulk (unstable) and interfaces (stable) of a QLL, Kuroda and Lacmann assumed that a QLL and an ice can be in equilibrium at the solid−vapor equilibrium water vapor pressure: a QLL can stably exist on an ice surface at equilibrium water vapor pressure. In addition,

taking into account the effects of kinetics, Kuroda and Lacmann also presumed that a QLL can exist under both undersaturated and supersaturated water vapor pressures. The reason why Kuroda and Lacmann felt justified in the assumption of complete wetting was mainly due to the overestimation of free energy of an ice−vapor interface.

B. Measurement of a focus depth of a Michelson interferometer

To evaluate a focus depth of a Michelson interferometer, we measured reflected light intensity I as a function of depth z (along the optical axis). Figure. B1 shows the results. At the position of z= 0, the focus was just set at a sample plane. The values of I were normalized by I at z= 0. Black circles show the experimental results. According to the imaging theory of confocal microcopy [75], the relation between I and z can be expressed as

$$I(z) = \left| \frac{\sin(kz)}{kz} \right|^2 . \qquad \text{(B1)}$$

Here, k is a constant 0.00975, determined by the wavelength, refractive indices, and the numerical aperture of the objective. Solid curves in Fig. B1 correspond to the theoretical fittings using eq. (B1). From Fig. B1, the focus depth of the Michelson interferometer (2.5-fold magnification) was estimated at 170 μm, at which position $I(z) = I(z = 0)/e$. Here, e is a base of natural logarithm.

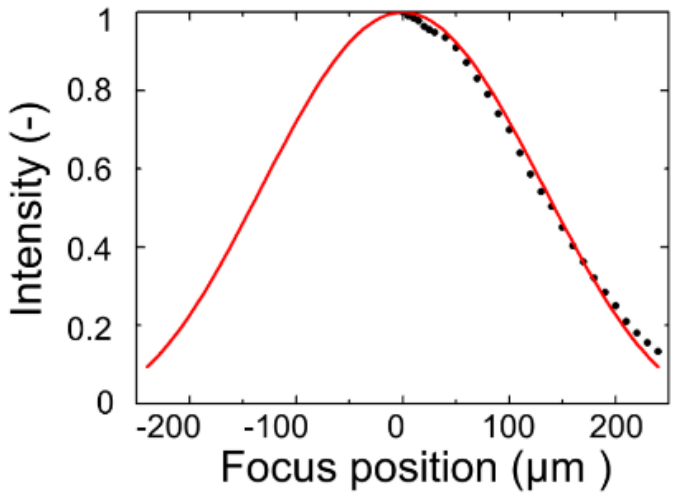

Fig. A1. Changes in intensity of reflected light (I) as a function of depth z (along the optical axis) when we used a Michelson interferometer (2.5-fold magnification). At the position of z= 0, the focus was just set at a sample plane. Black circles show experimental data, and a solid curve presents the theoretical fittings using eq. (B1).

C. Calculation of the temperature distribution

During the observation of a polycrystalline thin film, we separately control temperatures of an upper Cu plate T_{top} and a lower Cu plate T_{bottom}, of in the observation chamber. In this section, we explain the calculation of temperature distribution inside an observation chamber, in particular when T_{top} and T_{bottom} are significantly different.

C-1. A model and a calculation

For simplicity, we assume that the conduction of heat occurs in a one-dimensional (1D) way in the observation chamber. In a 1D system, a solution of a diffusion equation in a steady state shows a linear function. Hence, we assumed a linear temperature distribution as shown schematically in Fig. C1 when $T_{bottom} > T_{top}$. Since the heat conductivity of Cu is very high (k_{Cu}=403 ($W^{+1}m^{-1}k^{-1}$)), we assume that the temperature distribution inside the Cu plates is homogeneous. T and L show temperatures of interfaces and lengths of media, respectively: subscripts show their explanations. The values of heat conductivities of media k and their lengths L are summarized in Table C1. Here, T_{ice} corresponds to a real temperature of a polycrystalline ice thin film (T_{sample}) in the main text.

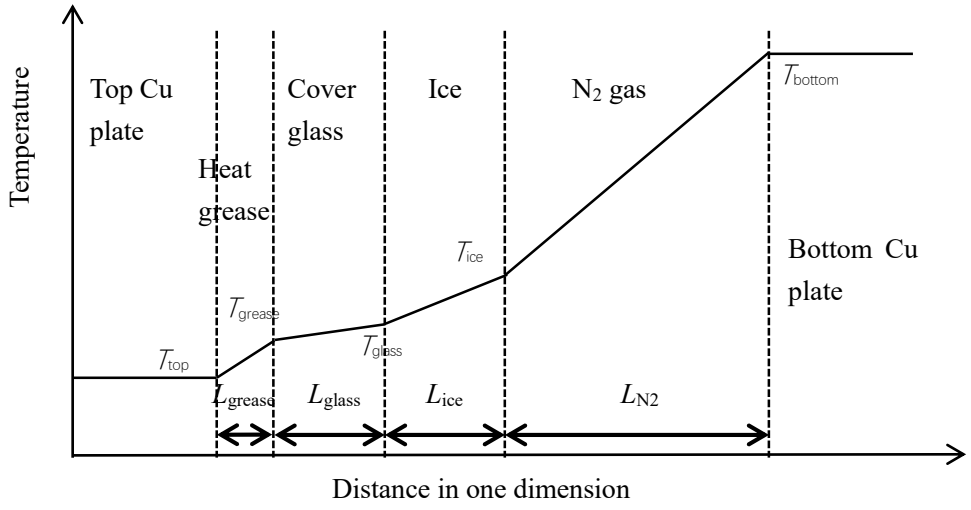

Fig. C1. Temperature distribution inside of an observation chamber. Heat conduction in one dimension is assumed. T and L denote temperatures at interfaces and lengths of media. Subscripts show explanations of the interfaces and the media.

Table C1 Heat conductivities and lengths of media

	Cu	Grease	Glass	Ice	N_2
Heat conductivity ($W^{+1}m^{-1}K^{-1}$= $J^{+1}m^{-1}K^{-1}$ s^{-1})	k_{Cu}=403	K_{grease}=0.21 (a value of epoxide regin is adopted)	K_{glass}=1.4 (a value of quartz glass is adopted)	K_{ice}=2.0	K_{N2}=0.0236
Length	-	L_{grease} =10 (μm) (just assumed)	L_{glass}=150 (μm)	L_{ice}=70 (μm)	L_{N2}=17.5 (mm)

Heat flux q ($W^{+1}m^{-2}$ = $J^{+1}m^{-2}s^{-1}$) in a medium is generally given by Fourier's law of heat flow:

$$q = -k\Delta T = -k\frac{dT}{dx}. \quad \text{(C1)}$$

By using eq. (C1), heat flux in the individual medium can be expressed as follows:

$$q_{N2} = -k_{N2}\frac{T_{bottom}-T_{ice}}{L_{N2}}, \quad \text{(C2-1)}$$

$$q_{ice} = -k_{ice}\frac{T_{ice}-T_{glass}}{L_{ice}}, \quad \text{(C2-2)}$$

$$q_{glass} = -k_{glass}\frac{T_{glass}-T_{grease}}{L_{glass}}, \quad \text{(C2-3)}$$

$$q_{grease} = -k_{grease}\frac{T_{grease}-T_{top}}{L_{grease}}. \quad \text{(C2-4)}$$

From eqs. (C2-1)-(C2-4), we obtained the followings.

$$-\frac{L_{N2}}{k_{N2}}\ q_{N2} = T_{bottom}-T_{ice}, \quad \text{(C3-1)}$$

$$-\frac{L_{ice}}{k_{ice}}\ q_{ice} = T_{ice}-T_{glass}, \quad \text{(C3-2)}$$

$$-\frac{L_{glass}}{k_{glass}}\ q_{glass} = T_{glass}-T_{grease}, \quad \text{(C3-3)}$$

$$-\frac{L_{grease}}{k_{grease}}\ q_{grease} = T_{grease}-T_{top}. \quad \text{(C3-4)}$$

In Fig. C1, since the heat conduction processes in each media are connected in series,

$$q_{N2} = q_{ice} = q_{glass} = q_{grease} = q. \quad \text{(C4)}$$

Then, calculate a sum of eqs. (C3-1) to (C3-4), and obtain

$-\left(\frac{L_{N2}}{k_{N2}} + \frac{L_{ice}}{k_{ice}} + \frac{L_{glass}}{k_{glass}} + \frac{L_{grease}}{k_{grease}}\right) q = T_{bottom} - T_{top}$, and then

$$-q = (T_{bottom} - T_{top}) / \left(\frac{L_{N2}}{k_{N2}} + \frac{L_{ice}}{k_{ice}} + \frac{L_{glass}}{k_{glass}} + \frac{L_{grease}}{k_{grease}}\right). \quad \text{(C5)}$$

In eq. (C5), $\left(\frac{L_{N2}}{k_{N2}} + \frac{L_{ice}}{k_{ice}} + \frac{L_{glass}}{k_{glass}} + \frac{L_{grease}}{k_{grease}}\right)$shows resistances (in series) to the heat conduction. From eq. (C5), we can obtain the heat flux q. Note that q has a negative sign.

After once we could obtain q, we can determine the temperatures at the interfaces from eq. (C3) as follows:

$$T_{ice} = T_{bottom} + \frac{L_{N2}}{k_{N2}} q, \quad \text{(C6-1)}$$

$$T_{glass} = T_{ice} + \frac{L_{ice}}{k_{ice}} q, \quad \text{(C6-2)}$$

$$T_{grease} = T_{glass} + \frac{L_{glass}}{k_{glass}} q. \quad \text{(C6-3)}$$

Here, also note that q has a negative sign. Hence, $T_{top} < T_{grease} < T_{glass} < T_{ice} < T_{bottom}$.

C-2. Evaluation of the temperature distribution

First, we set $T_{top} = -0.5$ °C and used the values of k and L shown in Table C1. Then, using eqs. (C5) and (C6), we determined the heat flux q and the interface temperatures T_{grease}, T_{glass}, and T_{ice}, as a function of T_{bottom}. Fig. C2 shows that the heat resistance of the nitrogen gas of 17.5 mm in length is extremely larger than the other resistances. Hence, even when $T_{bottom} = +100$ °C, $T_{ice} = -0.474$ °C. Now we fully neglect the heat conduction by the buoyancy-driven convection, hence we clearly overestimate the resistance of the nitrogen gas. However, under a realistic condition of $T_{bottom} = +1.0$ °C (in which the buoyancy-driven convection should be negligibly small), we can see $T_{top} = T_{grease} = T_{glass} = T_{ice} = -0.500$ °C (no difference with three significant digits). Therefore, we conclude that we can neglect the temperature gradient formed in the direction perpendicular to the sample surface.

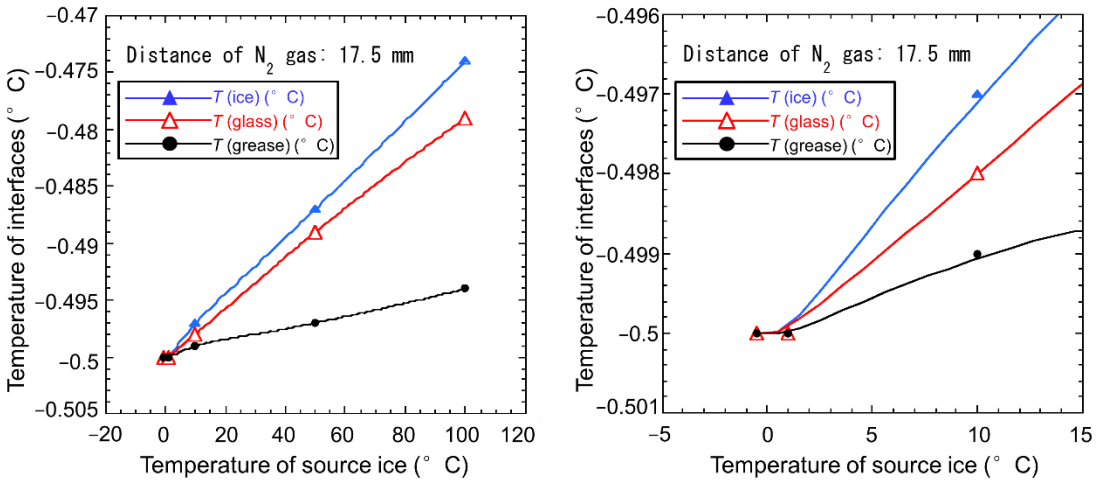

Fig. C2. Changes in the temperatures of the interfaces as a function of T_{bottom} (the temperature of the source ice).

We also estimated the effects of the length of the nitrogen gas phase on the heat conduction inside of the observation chamber. We set T_{top}= −0.5 °C and T_{bottom}= +1.0 °C, and calculated the temperatures of the interfaces as a function of the length of nitrogen gas phase L_{N2}. When L_{N2}=17.5 mm, $T_{top} = T_{grease} = T_{glass} = T_{ice}$ = −0.500 °C. However, when L_{N2}=1.75 and 0.175 mm, T_{ice} = −0.496 and −0.463 °C, respectively, as shown in Fig. C3. With decreasing distance L_{N2}, the heat resistance of the nitrogen gas decreases significantly, and hence T_{ice} increases. However, when L_{N2}>1 mm, the heat resistance of the nitrogen gas is enough large, and hence we can neglect the temperature gradient formed in the direction perpendicular to the sample surface (Fig. C3).

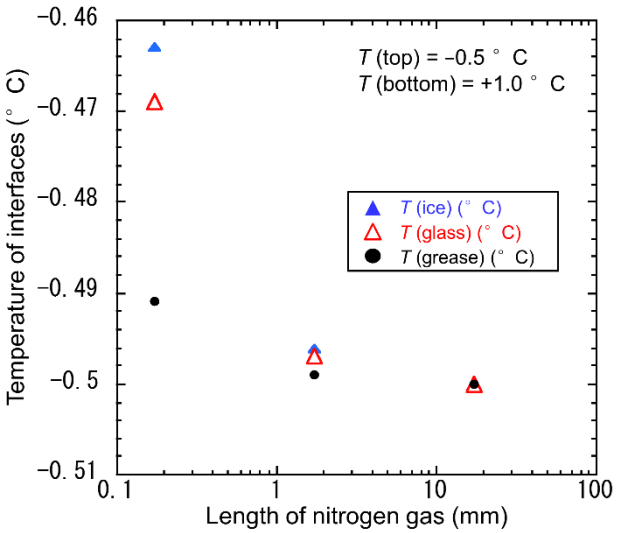

Fig. C3. Changes in the temperature if the interfaces as a function of the length of the nitrogen gas phase.

D. A list of publications and presentations

Publications

1. Jialu Chen, Ken Nagashima, Ken-ichiro Murata, Gen Sazaki, "Quasi-liquid layers can exist on polycrystalline ice thin films at a temperature significantly lower than on ice single crystals", Crystal Growth & Design, 19 (1), 116-124, 2019

2. Jialu Chen, Takao Maki, Ken Nagashima, Ken-ichiro Murata, and Gen Sazaki, "Correction to quasi-liquid layers can exist on polycrystalline ice thin films at a temperature significantly lower than on ice single crystals", Crystal Growth & Design, 20 (7), 4852-4854, 2020

3. Jialu Chen, Takao Maki, Ken Nagashima, Ken-ichiro Murata, and Gen Sazaki, "Quasi-liquid layers in grooves of grain boundaries and on grain surfaces of polycrystalline ice thin films", Crystal Growth & Design, 20 (11), 7188-7196, 2020

Conferences

a. International conferences

1. Jialu Chen, Ken Nagashima, Ken-ichiro Murata, Gen Sazaki, "Formation of quasi-liquid layers on polycrystalline ice", 14th International Conference on the Physics and Chemistry of Ice (PCI-2018 in Zürich), Paul Scherrer Institut, Zürich, Switzerland, January 8-12, 2018. (A poster presentation)

2. Jialu Chen, Ken Nagashima, Ken-ichiro Murata, Gen Sazaki, "Quasi-liquid layers on polycrystalline ice thin films", International Symposium & School on Crystal Growth Fundamentals, Convention Hall of Hotel Sakan, Akiu, Sendai, Japan, November 3-7, 2018. (A poster presentation)

3. Jialu Chen, Ken-ichiro Murata, Ken Nagashima, Gen Sazaki, "Quasi-Liquid Layers Can Exist on Polycrystalline Ice Thin Films at a Temperature Significant Lower than on Ice Single Crystals", 19th International Conference on Crystal Growth & Epitaxy,

International Conference Center, Keystone, Colorado, US, July 28- August 2, 2019. (An oral presentation)

b. Domestic conference

1. Jialu Chen, Ken Nagashima, Ken-ichiro Murata, Gen Sazaki, "Surface melting of polycrystalline ice", The Physical Society of Japan, 2017 Autumn Meeting, Iwate University, Morioka, September 21-24, 2017. (An oral presentation)

2. Jialu Chen, Ken Nagashima, Ken-ichiro Murata, Gen Sazaki, "Formation of quasi-liquid layers on polycrystalline ice", the 46th Japanese Conference on Crystal Growth, Hamamatsu, November 27-29, 2017. (An oral presentation)

3. Jialu Chen, Ken Nagashima, Ken-ichiro Murata, Gen Sazaki, "The temperature range of the existence of quasi-liquid layers on polycrystalline ice", The Physical Society of Japan, 73rd Annual Meeting, Tokyo University of Science, Tokyo, March 22-25, 2018. (An oral presentation)

4. Jialu Chen, Ken-ichiro Murata, Ken Nagashima, Gen Sazaki, "The emergence of quasi-liquid layers on polycrystalline ice thin films", The Physical Society of Japan, 2018 Autumn Meeting, Doshisha University, Kyoto, September 9-12, 2018. (An oral presentation)

5. Jialu Chen, Ken-ichiro Murata, Ken Nagashima, Gen Sazaki, "The appearance of quasi-liquid layers on polycrystalline ice thin films", the 47th Japanese Conference on Crystal Growth, Sendai, October 31-November 2, 2018. (An oral presentation)

6. Jialu Chen, Ken-ichiro Murata, Ken Nagashima, Gen Sazaki, "Liquid in grain boundaries of polycrystalline ice thin films", The Physical Society of Japan, 74th Annual Meeting, Kyushu University, Fukuoka, March 14-17, 2019. (An oral presentation)

7. Jialu Chen, Ken-ichiro Murata, Ken Nagashima, Gen Sazaki, "Behavior of QLLs on grain boundaries of polycrystalline ice thin films", the 48th Japanese Conference on Crystal Growth, Osaka University, October 30-November 1, 2019. (An oral

presentation)

8. Jialu Chen, Ken-ichiro Murata, Ken Nagashima, Gen Sazaki, "Surface melting of polycrystalline ice thin films Just below the melting point", The Physical Society of Japan, 2020 Autumn Meeting, Online, September 8-11, 2020. (An oral presentation)

Acknowledgements

I would like to express his sincere gratitude to Professor Dr. Gen Sazaki of Institute of Low Temperature Science, Hokkaido University, for his valuable suggestions and discussion, throughout this study in the last four years. His instruction has helped me to develop the scope of my knowledge to finish the research.

I also acknowledge Professor Dr. Akira Kouchi, Professor Dr. Naoki Watanabe, and Associate Professor Dr. Yuki Kimura of Institute of Low Temperature Science, Hokkaido University, for reading this thesis and for their many valuable suggestions.

I am very grateful to Dr. Ken Nagashima and Dr. Ken-ichiro Murata of Institute of Low Temperature Science, Hokkaido University, for providing helpful advice and discussions.

Reference

[1] M. Faraday, Lecture given at royal institution, june 7, 1850, reported in Athenaeum, London, 1850, pp. 640.

[2] J.G. Dash, A.W. Rempel, J.S. Wettlaufer, The physics of premelted ice and its geophysical consequences, Rev. Mod. Phys., **78** (2006) 695-741.

[3] J.G. Dash, Thermomolecular pressure in surface melting - motivation for frost heave, Science, **246** (1989) 1591-1593.

[4] J.S. Wettlaufer, J.G. Dash, Melting below zero, Sci. Am., **282** (2000) 50-53.

[5] R.R. Gilpin, Wire regelation at low-temperatures, J. Colloid Interface Sci., **77** (1980) 435-448.

[6] P. Sinha, S. Muralidharan, S. Sengupta, S. Veerappapillai, A brief review on antifreeze proteins: Structure, function and applications, **7** (2016) 914-919.

[7] W. Zhu, J. Guo, J.O. Agola, J.G. Croissant, Z. Wang, J. Shang, E. Coker, B. Motevalli, A. Zimpel, S. Wuttke, C.J. Brinker, Metal–organic framework nanoparticle-assisted cryopreservation of red blood cells, J. Am. Chem. Soc., **141** (2019) 7789-7796.

[8] V.F. Petrenko, R.W. Whitworth, Physics of ice, Oxford University Press, Oxford, 1999.

[9] V. Sadtchenko, G.E. Ewing, A new approach to the study of interfacial melting of ice: Infrared spectroscopy, Can. J. Phys., **81** (2003) 333-341.

[10] D. Beaglehole, D. Nason, Transition layer on the surface on ice, Surf. Sci., **96** (1980) 357-363.

[11] Y. Furukawa, M. Yamamoto, T. Kuroda, Ellipsometric study of the transition layer on the surface of an ice crystal, J. Cryst. Growth, **82** (1987) 665-677.

[12] I. Golecki, C. Jaccard, The surface of ice near 0°c studied by 100 kev proton channeling, Phys. Lett., **63A** (1977) 374-376.

[13] I. Golecki, C. Jaccard, Intrinsic surface disorser in ice near the melting point, J. Phys. C: Solid State Phys., **11** (1978) 4229.

[14] A. Kouchi, Y. Furukawa, T. Kuroda, X-ray diffraction pattern of quasi-liquid layer on ice crystal surface, JPhys, **48** (1987) 675-677.

[15] D. Nasson, N.H. Fletcher, Photoemission from ice and water surfaces: Quasiliquid layer effect, J. Chem. Phys., **62** (1975) 4444-4449.

[16] H. Bluhm, D.F. Ogletree, C.S. Fadley, Z. Hussain, N. Salmeron, The premelting of ice studied with photoelectron spectroscopy, Journal of Physics-Condensed Matter, **14** (2002) L227-L233.

[17] A. Doppenschmidt, H.J. Butt, Measuring the thickness of the liquid-like layer on ice surfaces with atomic force microscopy, Langmuir, **16** (2000) 6709-6714.

[18] H. Bluhm, M. Salmeron, Growth of nanometer thin ice films from water vapor studied using scanning polarization force microscopy, J. Chem. Phys., **111** (1999) 6947-6954.

[19] B. Pittenger, S.C. Fain, M.J. Cochran, J.M.K. Donev, B.E. Robertson, A. Szuchmacher, R.M. Overney, Premelting at ice-solid interfaces studied via velocity-dependent indentation with force microscope tips, PhRvB, **63** (2001).

[20] M. Salmeron, H. Bluhm, Structure and properties of ice and water film interfaces in equilibrium with vapor, Surf. Rev. Lett., **6** (1999) 1275-1281.

[21] V.F. Petrenko, Study of the surface of ice, ice/solid and ice/liquid interfaces with scanning force microscopy, J. Phys. Chem. B, **101** (1997) 6276-6281.

[22] M.P. Goertz, X.Y. Zhu, J.E. Houston, Exploring the liquid-like layer on the ice surface, Langmuir,

25 (2009) 6905-6908.
[23] H. Dosch, A. Lied, J.H. Bilgram, Glancing-angle x-ray scattering studies of the premelting of ice surfaces, Surf. Sci., **327** (1995) 145-164.
[24] H. Dosch, A. Lied, J.H. Bilgram, Disruption of the hydrogen-bonding network at the surface of i-h ice near surface premelting, Surf. Sci., **366** (1996) 43-50.
[25] M. Elbaum, S.G. Lipson, J.G. Dash, Optical study of surface melting on ice, J. Cryst. Growth, **129** (1993) 491-505.
[26] R.R. Gilpin, Theoretical studies of particle engulfment, J. Colloid Interface Sci., **74** (1980) 44-63.
[27] T. Ishizaki, M. Maruyama, Y. Furukawa, J.G. Dash, Premelting of ice in porous silica glass, J. Cryst. Growth, **163** (1996) 455-460.
[28] L.A. Wilen, J.G. Dash, Frost heave dynamics at a single crystal interface, Phys. Rev. Lett., **74** (1995) 5076-5079.
[29] R. Lacmann, I.N. Stranski, The growth of snow crystals, J. Cryst. Growth, **13-14** (1972) 236-240.
[30] T. Kuroda, R. Lacmann, Growth kinetics of ice from the vapor phase and its growth forms, J. Cryst. Growth, **56** (1982) 189-205.
[31] Y. Furukawa, Snow and ice crystal growth, 2015, pp. 1061-1112.
[32] Z. Chen, y.-r. Shen, G. Somorjai, Studies of polymer surfaces by sum frequency generation vibrational spectroscopy, Annu. Rev. Phys. Chem., **53** (2002) 437-465.
[33] X. Wei, P.B. Miranda, Y.R. Shen, Surface vibrational spectroscopic study of surface melting of ice, Phys. Rev. Lett., **86** (2001) 1554-1557.
[34] H. Groenzin, I. Li, V. Buch, M.J. Shultz, The single-crystal, basal face of ice ih investigated with sum frequency generation, The Journal of Chemical Physics, **127** (2007) 214502.
[35] H. Groenzin, I. Li, M.J. Shultz, Sum-frequency generation: Polarization surface spectroscopy analysis of the vibrational surface modes on the basal face of ice ih, The Journal of Chemical Physics, **128** (2008) 214510.
[36] I. Li Barnett, H. Groenzin, M.J. Shultz, Hydrogen bonding in the hexagonal ice surface, The Journal of Physical Chemistry A, **115** (2011) 6039-6045.
[37] P.J. Bisson, M.J. Shultz, Hydrogen bonding in the prism face of ice ih via sum frequency vibrational spectroscopy, The Journal of Physical Chemistry A, **117** (2013) 6116-6125.
[38] Y. Nagata, T. Hasegawa, E.H.G. Backus, K. Usui, S. Yoshimune, T. Ohto, M. Bonn, The surface roughness, but not the water molecular orientation varies with temperature at the water–air interface, PCCP, **17** (2015) 23559-23564.
[39] W.J. Smit, F.J. Tang, M.A. Sanchez, E.H.G. Backus, L.M. Xu, T. Hasegawa, M. Bonn, H.J. Bakker, Y. Nagata, Excess hydrogen bond at the ice-vapor interface around 200 k, Phys. Rev. Lett., **119** (2017) 133003-133001-133005.
[40] G. Sazaki, T. Matsui, K. Tsukamoto, N. Usami, T. Ujihara, K. Fujiwara, K. Nakajima, In situ observation of elementary growth steps on the surface of protein crystals by laser confocal microscopy, J. Cryst. Growth, **262** (2004) 536-542.
[41] G. Sazaki, S. Zepeda, S. Nakatsubo, E. Yokoyama, Y. Furukawa, Elementary steps at the surface of ice crystals visualized by advanced optical microscopy, Proc. Natl. Acad. Sci. U.S.A., **107** (2010) 19702-19707.
[42] G. Sazaki, S. Zepeda, S. Nakatsubo, M. Yokomine, Y. Furukawa, Quasi-liquid layers on ice

crystal surfaces are made up of two different phases, Proc. Natl. Acad. Sci. U.S.A., **109** (2012) 1052-1055.

[43] K. Murata, H. Asakawa, K. Nagashima, Y. Furukawa, G. Sazaki, In situ determination of surface tension-to-shear viscosity ratio for quasiliquid layers on ice crystal surfaces, Phys. Rev. Lett., **115** (2015).

[44] H. Asakawa, G. Sazaki, K. Nagashima, S. Nakatsubo, Y. Furukawa, Prism and other high-index faces of ice crystals exhibit two types of quasi-liquid layers, Cryst. Growth Des., **15** (2015) 3339-3344.

[45] G. Sazaki, H. Asakawa, K. Nagashima, S. Nakatsubo, Y. Furukawa, How do quasi-liquid layers emerge from ice crystal surfaces?, Cryst. Growth Des., **13** (2013) 1761-1766.

[46] K. Murata, H. Asakawa, K. Nagashima, Y. Furukawa, G. Sazaki, Thermodynamic origin of surface melting on ice crystals, Proc. Natl. Acad. Sci. U.S.A., **113** (2016) E6741-E6748.

[47] H. Asakawa, G. Sazaki, K. Nagashima, S. Nakatsubo, Y. Furukawa, Two types of quasi-liquid layers on ice crystals are formed kinetically, Proc. Natl. Acad. Sci. U.S.A., **113** (2016) 1749-1753.

[48] H. Asakawa, G. Sazaki, E. Yokoyama, K. Nagashima, S. Nakatsubo, Y. Furukawa, Roles of surface/volume diffusion in the growth kinetics of elementary spiral steps on ice basal faces grown from water vapor, Cryst. Growth Des., **14** (2014) 3210-3220.

[49] M. Inomata, K. Murata, H. Asakawa, K. Nagashima, S. Nakatsubo, Y. Furukawa, G. Sazaki, Temperature dependence of the growth kinetics of elementary spiral steps on ice basal faces grown from water vapor, Cryst. Growth Des., **18** (2018) 786-793.

[50] H.M. Mader, Observation of the water-vein system in polycrystalline ice, Journal of Glaciology, **38** (1992) 333-347.

[51] H.M. Mader, The thermal-behavior of the water-vein system in polycrystaline ice, Journal of Glaciology, **38** (1992) 359-374.

[52] H. Lu, S.A. McCartney, V. Sadtchenko, Fast thermal desorption spectroscopy study of h/d isotopic exchange reaction in polycrystalline ice near its melting point, J. Chem. Phys., **127** (2007).

[53] E.S. Thomson, J.S. Wettlaufer, L.A. Wilen, A direct optical method for the study of grain boundary melting, Review of Scientific Instruments, **80** (2009) 103903-103901-103907.

[54] E.S. Thomson, H. Hansen-Goos, J.S. Wettlaufer, L.A. Wilen, Grain boundary melting in ice, Journal of Chemical Physics, **138** (2013) 124707-124701-124705.

[55] L. Benatov, J.S. Wettlaufer, Abrupt grain boundary melting in ice, Physical Review E, **70** (2004) 061606-061601-061607.

[56] E.S. Thomson, L. Benatov, J.S. Wettlaufer, Abrupt grain boundary melting in ice (vol 70, 061606, 2004), Physical Review E, **82** (2010) 039907-039901.

[57] J. Chen, T. Maki, K. Nagashima, K.-i. Murata, G. Sazaki, Correction to quasi-liquid layers can exist on polycrystalline ice thin films at a temperature significantly lower than on ice single crystals, Cryst. Growth Des., **20** (2020) 4852-4854.

[58] J.S. Sterinhart, S.R. Hart, Calibration curves for thermistors, Deep-Sea Research, **15** (1968) 497-503.

[59] D. Sonntag, Important new values of the physical constants of 1986, vapour pressure formulations based on the its-90, and psychrometer formulae, Meteorol Z, **70** (1990) 340-344.

[60] D.M.K. Murphy, T., Review of the vapour pressures of ice and supercooled water for

atmospheric applications, QJRMS, **131** (2005) 1539-1565.
[61] D.G. Brandon, B. Ralph, S. Ranganathan, M.S. Wald, Field ion microscope study of atomic configuration at grain boundaries, Acta Metall., **12** (1964) 813-821.
[62] C.L. Vold, M.E. Glicksman, Behavior of grain boundaries near the melting point, in: H. Hu (Ed.) The nature and behavior of grain boundaries: A symposium held at the tms-aime fall meeting in detroit, michigan, october 18–19, 1971, Springer US, New York, NY, 1972, pp. 171-183.
[63] T. Watanabe, An approach to grain-boundary design for strong and ductile polycrystals, Res Mechanica, **11** (1984) 47-84.
[64] A. Higashi, Structure and behaviour of grain boundaries in polycrystalline ice, JGlac, **21** (1978) 589-605.
[65] T. Hondoh, A. Higashi, X-ray diffraction topographic observations of the large-angle grain boundary in ice under deformation, JGlac, **21** (1978) 629-638.
[66] T. Hondoh, A. Higashi, Anisotopy of migration and faceting of large-angle grain boundaries in ice bicrystals, Philos. Mag. A, **39** (1979) 137-149.
[67] E.S. Thomson, J.S. Wettlaufer, L.A. Wilen, A direct optical method for the study of grain boundary melting, Rev. Sci. Instrum., **80** (2009).
[68] E.S. Thomson, H. Hansen-Goos, J.S. Wettlaufer, L.A. Wilen, Grain boundary melting in ice, The Journal of Chemical Physics, **138** (2013) 124707.
[69] A. Dehaoui, B. Issenmann, F. Caupin, Viscosity of deeply supercooled water and its coupling to molecular diffusion, Proc. Natl. Acad. Sci. U.S.A., **112** (2015) 12020.
[70] E. Yokoyama, I. Yoshizaki, T. Shimaoka, T. Sone, T. Kiyota, Y. Furukawa, Measurements of growth rates of an ice crystal from supercooled heavy water under microgravity conditions: Basal face growth rate and tip velocity of a dendrite, The Journal of Physical Chemistry B, **115** (2011) 8739-8745.
[71] D. Rozmanov, P.G. Kusalik, Anisotropy in the crystal growth of hexagonal ice, ih, The Journal of Chemical Physics, **137** (2012) 094702.
[72] J.S. Wettlaufer, M.G. Worster, Premelting dynamics, AnRFM, **38** (2006) 427-452.
[73] Y. Suzuki, G. Sazaki, K. Hashimoto, T. Fujiwara, Y. Furukawa, Colloidal crystallization utilizing interfaces of unidirectionally growing ice crystals, J. Cryst. Growth, **383** (2013) 67-71.
[74] A.A. Chernov, Modern crystallography iii, Springerr-Verlag, Berlin, 1984.
[75] T.R. Corle, G.S. Kino, Confocal scanning optical microscopy and related imaging systems, Academic Press, London, 1996.